Seasonal $\delta^{18}O$ Signals in Greenland Ice Cores

Bo Møllesøe Vinther

Speciale

Vejledere:
Katrine Krogh Andersen
Aksel Walløe Hansen

Geofysisk Afdeling
Niels Bohr Institutet
for Astronomi, Fysisk
og Geofysik

Københavns Universitet

2. udgave

3. september 2003

Abstract

Methods for recovering seasonal stable isotope signals from ice cores are developed and presented. This includes the development of an improved simple flow model for large ice sheets as well as a thorough analytical as well as numerical analysis of stable isotope diffusion in ice sheets.

Using ice cores with medium to high accumulation rates from the southern half of the Greenland ice sheet it is possible to recover seasonal isotope variations. The seasonally resolved stable isotope data opens a range of interesting possibilities.
Winter season stable isotope data are very well correlated to Greenland west coast winter temperatures and the North Atlantic Oscillation (NAO). Hence from the Greenland ice sheet it may be possible to extract highly resolved information on the NAO during the entire Holocene period.
Summer season stable isotope data are well correlated to Greenland east coast and Icelandic summer temperatures. The climate at these locations is strongly influenced by North Atlantic sea surface temperatures and sea ice conditions. Hence significant correlations between summer season stable isotope data and sea surface temperatures in Greenland and Icelandic waters are also observed. It is therefore speculated that summer ice core data could provide highly resolved information on the state of the North Atlantic during the Holocene.

Acknowledgements

First of all I would like to thank my supervisors Katrine K. Andersen and Aksel W. Hansen from the Department of Geophysics, NBIfAFG. The thesis would not have been finished on time, if it wasn't for all the help and encouragement provided by Katrine during the last month of the writing. Katrine also initiated the work with the paper on winter season ice core data, which is now published and in fact gave the foundation for this thesis. Aksel helped a lot with the more meteorological aspects of the paper.
I would also like to thank Sigfús J. Johnsen for all the long and fruitful discussions on diffusion correction of ice core data. And during the first few months after I started to look at the seasonal ice core data Sigfús provided me with diffusion corrected data whenever I needed them, even by mail at 2 a.m. in the morning! I simply cannot thank Sigfús enough. When I needed some details concerning the ice cores the office of Henrik B. Clausen was always open. I would also like to thank Henrik for all his help with the dating of the ice cores.
A quite substantial amount of meteorological data has been collected for this thesis. I am deeply grateful for all the help and encouragement I have received during this process. Hence I would like to thank the staff at the Danish Meteorological Institute library for their guidance on old Greenland temperature data, Poul Frich for providing me with the old weather observations from Danish naval vessels, Knud Frydendahl and Eigil Kaas for their help in locating Poul Frich and thereby the old observations.
Michael Petersen and Martin Zedeler helped me get rid of a lot of errors in the last week or two before the deadline. All remaining errors are probably introduced by my own last minute corrections.
Finally I would like to thank my family: Ellen, Joachim, Anders, Trine and Naja for their help and understanding especially during the last month of the writing. Ellen and Joachim even invited both me and my computer on a splendid summer holiday in France.

Second Edition

This is the second edition of my masters thesis (speciale), which was submitted for evaluation on August the 18th 2003. The only changes made in the second edition are the correction of some grammatical errors and a few typing errors.

Contents

Chapter 1

Introduction

Climate change has become a major scientific as well as a political issue during the past two decades. Enormous efforts are being made all over the world to better understand global climate and ascertain to which degree human activities influence the climate system.
It is becoming more and more clear, that in order to understand global climate variability one has to have extensive knowledge of regional scale variability as well.
Indeed Jones et al. [2001] stressed the necessity of having millennial scale seasonally resolved regional information on climate variability. Without such detailed information it will not be possible to separate natural climate variability from a possible human caused effect.
Unfortunately meteorological observations with global coverage have only been carried out routinely for about half a century. For Europe, which is the region with the longest records of observations, two centuries of climate variability are known [Jones et al. 1999 a].
Studying natural proxies for climate variability, such as data based on tree ring measurements, analysis of ocean sediment cores, corals or ice cores are therefore the only way to obtain millennial scale climatic information.
There is however the caveat that most natural proxies only have annual or decadal resolution; thus not optimally fulfilling the demands of the scientific community of seasonally resolved data.

Stable isotopes in ice cores have long been known to be a useful proxy for atmospheric temperature [Dansgaard, 1964]. During the past decade some efforts have been made to relate seasonal Greenland ice core stable isotope data to seasonal climatic variability [Barlow et al., 1993; 1997; Rogers et al., 1998].
The seasonally resolved stable isotope data from Greenland, which were used in these investigations did however have a quite small signal to noise ratio. Hence only weak relations between seasonal climate and the ice core data were found.

In a paper made as a part of the initial research for this thesis [Vinther et al. 2003 a] (also appendix A) winter season stable isotope data from multiple ice cores (most with a relatively high data signal to noise ratio) were found to relate strongly to Greenland winter temperatures.
The Vinther et al. [2003 a] paper also found significant relations between the winter season ice core data and the most prominent pattern of northern hemisphere (NH) atmospheric variability the North Atlantic Oscillation (NAO) [Hurrel et al., 2003].

The NAO is commonly described in terms of seesaws of pressure and temperature. The pressure seesaw is between the Icelandic and the Azores region. When Icelandic pressure is lower than normal, then the pressure at the Azores will tend to be higher than normal and the NAO is said to be in the high index mode. In the case of higher than normal Icelandic pressure the Azores pressure will tend to be lower than normal and the NAO is in low index mode.
The NAO temperature seesaw is present during the extended winter season (Nov-Apr) and is a consequence of the atmospheric flow pattern associated with the pressure seesaw. In the high index mode flow from north over Greenland will increase and Greenland temperatures will therefore decrease (see figure 1.1). When the NAO is in high index mode there will also be an increase in westerly flow over north-west Europe bringing with it mild Atlantic air. Hence Greenland will be cooler than normal while north-western

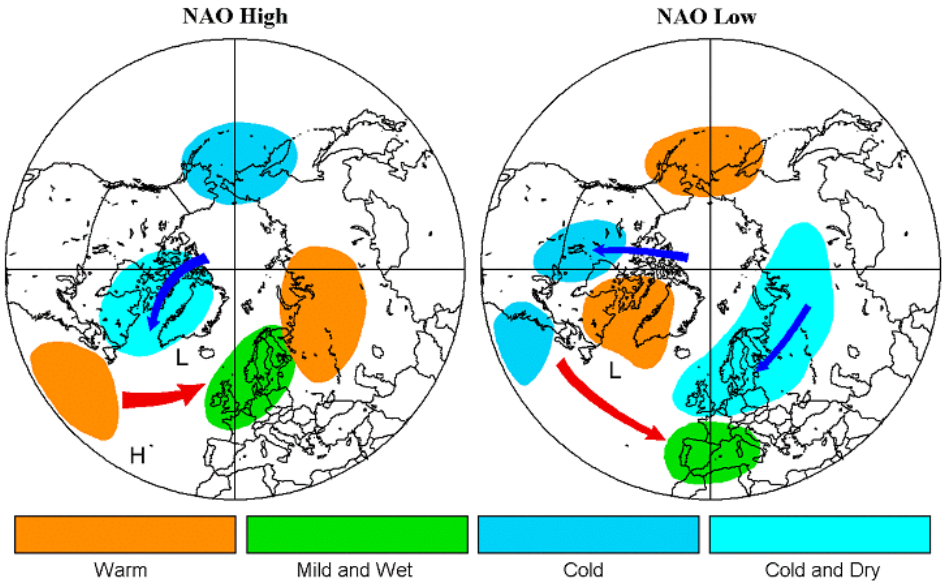

Figure 1.1: Schematic view of NAO influence on NH winter weather. For further details see the main text. Figure is from Hansen et al. [2001].

Europe will be warmer than normal in a NAO high index winter.
From figure 1.1 it can be seen that the opposite is the case when the NAO is in low index mode. The temperature seesaw is therefore said to be between north-western Europe and Greenland.
When studying figure 1.1 it is however clear that huge areas around the NH is affected by the NAO. This underlines the importance of the NAO for NH climate.
The great influence of the NAO on Greenland winter temperatures explains the relation between the NAO and Greenland ice core data from the winter season. The ice core stable isotopes recording the NAO related temperature differences in Greenland winter temperatures.

This thesis should be viewed as an extension of the initial work presented in the Vinther et al. [2003 a] paper. Now both winter and summer season stable isotope data will be examined instead of winter data only. Further, more ice core data will be examined here than in the initial paper. Finally this thesis will present an analysis of the glaciological issues of importance for the seasonal stable isotope signals. A subject not covered by the Vinther et al. [2003 a] paper.

The thesis is structured in the following manner:

Chapter 2 introduces the ice core data.
Chapter 3 threats the topic of diffusion of stable isotopes in snow and ice. In this chapter an improved ice flow model will be introduced. This model will pave the way for a deduction of a new set of equations quantifying stable isotope diffusion.
Chapter 4 is devoted to the issues concerning the practical numerical calculations involved in retrieving the seasonal stable isotope data. In this chapter methods to diffusion correct and evaluate noise levels in ice core stable isotope data will be derived.
Chapter 5 is concerned with relations between seasonal Greenland temperatures and the seasonal Greenland ice core stable isotope data. Here comparisons between the ice core data and more than a hundred years of temperature observations will be carried out.
Chapter 6 investigates relations between the seasonal stable isotope data and north Atlantic region atmospheric flow as well as oceanic temperatures of the region.
Chapter 7 examines the stability of the most important relations found in chapter 6. The NAO signal in the winter season stable isotopes will be further investigated using data from the Vinther et al., [2003 a] paper.
Chapter 8 discusses remaining problems contra what have been achieved in this thesis.
Chapter 9 presents the main conclusions of this thesis.
The paper which was the result of the initial investigation into the seasonal

ice core data [Vinther et al., 2003 a] is reprinted in **Appendix A**. A number of issues of a more descriptive nature were deferred to the **Appendices B, C, and D** at the end of the thesis.

Chapter 2

The Ice Core Data

The vast Antarctic and Greenland ice sheets are outstanding archives of past atmospheric conditions. They consist of layer upon layer of snow and ice, all stemming from snow settling on the surface of the ice sheets during the past thousands or even hundreds of thousands of years.
The oldest ice layers will be near the bottom of an ice sheet while the youngest layers consist of recently precipitated snow near the surface. Hence a core drilled down through an ice sheet, from top to bottom, will provide a chronology past precipitation.
The number of years such a chronology spans will depend on the annual amount of snow precipitating on the ice sheet. Hence a core drilled through the Antarctic ice sheet, where precipitation generally is scarce will provide a very long chronology.
Where precipitation is plentiful, ice core chronologies will span much fewer years as each annual layer will be thicker. Thick annual layers will however contain detailed information about seasonal or even monthly atmospheric conditions. Information not preserved in thin annual layers.
While precipitation over Antarctica is very modest, large areas of the Greenland ice sheet enjoys sufficient amounts of precipitation for information on seasonal atmospheric conditions to be preserved.
This survey focuses exactly on such seasonal information. Therefore only ice cores from the Greenland ice sheet will be investigated.

2.1 Stable isotopes in ice cores

In this survey the main focus will be on the abundances of the ^{16}O and ^{18}O stable isotopes in the ice cores. What makes these stable isotopes of particular interest is the fact that their relative abundance in an air mass is temperature dependent [Dansgaard, 1964]. The heavy isotope, when being part of a water molecule ($H_2^{18}O$), condenses and precipitates with slightly more ease than does the $H_2^{16}O$ water molecule. Hence as air cools and water condenses and precipitates, the abundance of $H_2^{18}O$ relative to $H_2^{16}O$ in the

air decreases.
The ^{18}O to ^{16}O ratio in snow precipitating on the Greenland ice sheet can therefore be used as a proxy for Greenland temperature provided water evaporates with a constant ^{18}O to ^{16}O ratio at the source. As the Greenland precipitation originates mainly from evaporation over the subtropical North Atlantic this assumption seems to hold [Johnsen and White, 1989].
In a mass spectrometer one measures the deviation of the ^{18}O to ^{16}O ratio from a standard instead of the ratio itself. Hence the usual information available is the ^{18}O to ^{16}O ratio in a given ice core sample as compared to the ^{18}O to ^{16}O ratio in Standard Mean Ocean Water (SMOW):

$$\delta^{18}O = \frac{\left(\frac{^{18}O}{^{16}O}\right) - \left(\frac{^{18}O}{^{16}O}\right)_{SMOW}}{\left(\frac{^{18}O}{^{16}O}\right)_{SMOW}} \cdot 1000‰ \tag{2.1}$$

Hence low values of $\delta^{18}O$ imply small ^{18}O to ^{16}O ratios suggesting low temperatures while a higher value of $\delta^{18}O$ implies a larger ^{18}O to ^{16}O ratio suggesting a higher temperature.
Considering the Greenland ice sheet, the relationship between $\delta^{18}O$ and temperature is remarkably solid. Plotting mean ice core $\delta^{18}O$ versus surface temperatures at the corresponding drill sites, Dansgaard et al. [1973] found an impressively strict linear relationship.
Seasonal variations in $\delta^{18}O$ are also observed in ice cores. The annual temperature cycle gives rise to a strong annual cycle in ice core $\delta^{18}O$. In fact counting annual $\delta^{18}O$ cycles down through an ice core is very helpful when trying to estimate the age of a given core layer.
When studying ice core $\delta^{18}O$ values there is however a problem one has to bear in mind. The $\delta^{18}O$ data are biased by accumulation. That is to say the $\delta^{18}O$ values in the ice cores originate from a number of precipitation events. If a winter has no precipitation, it will not be recorded in the ice core $\delta^{18}O$ data at all. This is of course a minor problem when studying $\delta^{18}O$ data on long time scales (decades or longer), but looking at seasonal data it is very important to consider this bias.

2.2 Noise in the stable isotope data

Ice core $\delta^{18}O$ data are known to contain significant amounts of non-climatic variations. This is mainly due to the following processes [Fisher et al., 1996]:

- Post depositional wind driven redistribution of snow. The snow blowing from local high areas and later resettling in lower areas.
- As the snow sinks down through the ice sheet it gets denser and some mixing takes place.

- Summer melting at low altitude sites is responsible for some vertical redistribution.
- Diffusion especially in the top $\sim 70m$ of the ice sheet tends to smoothen the $\delta^{18}O$ data.

All these non-climatic variations are of course not welcome when trying to use $\delta^{18}O$ data to retrieve climatic information and they are generally considered as noise.
One way to reduce the noise introduced by blowing snow and resettling during densification is to make means of $\delta^{18}O$ spanning long time sections of an ice core. This approach however typically reduces the $\delta^{18}O$ time resolution to a scale of decades.
Therefore the only way to reduce the noise while maintaining seasonal resolution in the $\delta^{18}O$ data is to drill multiple ice cores at a given location and then stack the data in order to increase the signal to noise ratio. It should be noted however, that cores should be drilled more than 10 meters apart to avoid having the same post depositional noise in the cores [Fisher et al., 1996].
With respect to melt layers, it is possible to find high altitude drill sites on the Greenland ice sheet where temperatures are almost always below freezing and hence to avoid the problem.
As most diffusive processes concerning $\delta^{18}O$ in ice sheets are well understood, it is possible to correct the data for diffusion. This quite complicated subject will be treated thoroughly in the following chapter.

2.3 The Greenland ice cores

The ice cores selected for this study are all from areas of the Greenland ice sheet with medium to high accumulation. A choice being based on the fact that for accumulation rates below 0.2 meters of ice equivalent per year all seasonal information in the $\delta^{18}O$ data will be obliterated by diffusion [Johnsen et al., 1999]. Further it was decided to restrict the survey to ice core records spanning a minimum of some 200 years, as a significant number of climatic observations are available for comparison with the ice core data for the last two centuries.
Finally a few ice cores from north west Greenland (Camp Century) were left out as the accumulation was very inhomogeneous in its distribution over different years, thus making interpretation of the seasonal $\delta^{18}O$ data impossible.
Details concerning the ice cores selected for this survey are presented in the tables 2.1 and 2.2. Locations of the main Greenland ice core drill sites used here are shown on figure 2.1.

Table 2.1: Ice core drill site locations and core details.[a]

Drill site	Lat. $^\circ N$	Long. $^\circ W$	Elevation m a.s.l.	Drill year	Core length m
Crete	71.12	37.32	3172	1974	404.0
Dye 3 71	65.18	43.83	2480	1971	372
Dye 3 79	65.18	43.83	2480	1979[b]	2037
Dye 3 4B	65.17	43.93	2491	1983	173.8
Dye 3 18C	65.03	44.39	2620	1984	113.0
GRIP 89-1	72.58	37.64	3238	1989	260.1
GRIP 89-3	72.58	37.64	3238	1989[b]	3028.8
GRIP 91	72.58	37.64	3238	1991	82.3
GRIP 92	72.58	37.64	3238	1992	107.3
GRIP 93	72.58	37.64	3238	1993	229.5
Milcent	70.30	44.50	2410	1973	398
Site A	70.63	35.82	3092	1985	128.6
Site B	70.65	37.48	3138	1984	105.6
Site D	70.64	39.62	3018	1984	100.1
Site E	71.76	35.85	3087	1985	77.8
Site G	71.15	35.84	3098	1985	70.8

[a]Data sources are: [Langway et al., 1985; Clausen et al., 1988; Clausen and Hammer, 1988; Dansgaard et al, 1993].

[b]Cores were drilled to bedrock during a few years of fieldwork.

Table 2.2: Ice core drill site meteorological parameters.

Drill site	Pressure[a] hPa	Temperature at 10m[b] $^{\circ}C$	Accumulation rate m(ice)/yr
Crete	669	-31.4	0.289
Dye 3 71/79	736	-20.0	0.535
Dye 3 4B	735	-	0.535[c]
Dye 3 18C	722	-	0.440[c]
GRIP	663	-32.0	0.230
Milcent	744	-22.3	0.540
Site A	677	-29.4	0.292[c]
Site B	672	-29.8	0.306[c]
Site D	684	-28.3	0.354[c]
Site E	677	-30.4	0.215[c]
Site G	676	-30.1	0.249[c]

[a]Pressure data are derived from Greenland automatic weather station data using the hydrostatic approximation - see Appendix C.
[b]Sources for temp. data: [Clausen et al., 1988; Clausen and Hammer, 1988; Dansgaard et al, 1993].
[c]Accumulation rates calculated using measured density profiles and depths of the Laki volcanic erruption (1783 A.D.) from [Clausen and Hammer, 1988].

Figure 2.1: Location of Greenland drill sites.

Chapter 3

Diffusion of Stable Isotopes in Firn and Ice

To properly interpret a stable isotope ice core record it is necessary to consider diffusive processes that take place after snow deposition. As time goes by the snow densifies and slowly sinks down into the ice sheet. During the densification a considerable diffusive smoothing of the originally deposited stable isotope signal is observed. Hence summer and winter excursions in the stable isotope data are damped (see figure 3.1). When interpreting seasonal scale climate signals in stable isotope records it is therefore vital to take post depositional diffusion into account.
The approach here will be to reconstruct the original signal as it would have been just after deposition from the ice core records. This method has been continuously developed during the last 25 years, the first paper [Johnsen, 1977] establishing the basic physical and mathematical approach.
Johnsen [1977] introduced the following two fundamental equations for reconstructing the original stable isotope signal from ice core isotope data:

$$A_0 = A e^{\frac{1}{2}k^2\sigma^2} \tag{3.1}$$

$$\frac{d\sigma^2}{dt} = 2\dot{\varepsilon_z}\sigma^2 + 2\Omega \tag{3.2}$$

The first equation gives the original amplitude A_0 of a harmonic signal with wave number k and amplitude A in the stable isotope data. Thus by calculating the fourier components of the stable isotope signal in the ice core data, (3.1) can be used to derive the original amplitudes of the components. Thereafter the amplitude corrected fourier components can be used to reconstruct the original signal. In (3.1) it is however necessary to have knowledge of the diffusion length σ, which varies down through the ice sheet. Here the second equation is needed. The differential equation (3.2) has to be solved in order to obtain the diffusion length. As this involves knowledge of the

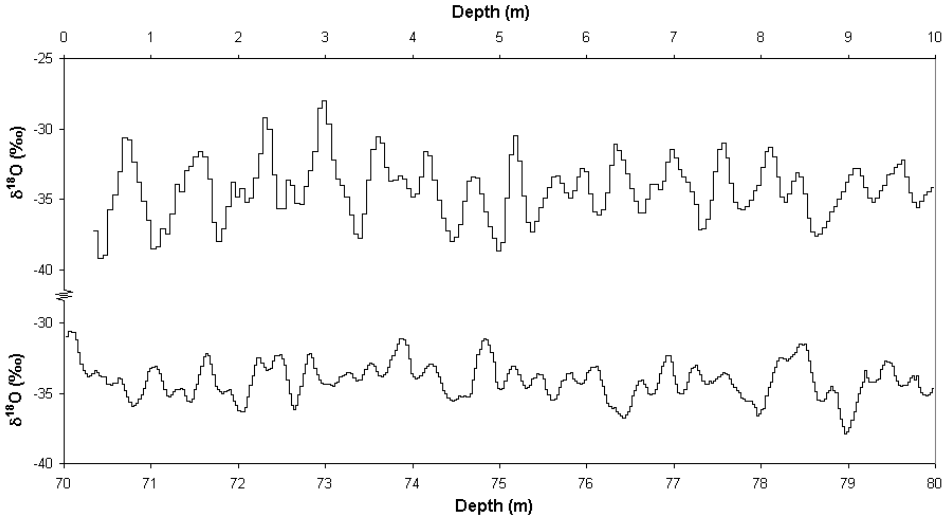

Figure 3.1: Detailed $\delta^{18}O$ profiles from two different levels in the Crete ice core.

vertical strain rate $\dot{\varepsilon_z}$ in the ice sheet, models of ice flow and densification have to be used. Further the diffusivity Ω has to be determined from the physical properties of the ice, which also depends on ice density.
Recently Johnsen et al. [2000] revisited the subject and included new understanding of diffusive processes as well as densification processes in the diffusion length calculations. The derivation of diffusion lengths presented here owes much to this recent paper.
As extensive use of ice flow and densification modelling is crucial for deriving the diffusion lengths, the following sections will be used to introduce these basic issues.

3.1 Densification of firn and ice

The process transforming snow precipitated onto the surface of an ice sheet into solid ice can be divided into three stages [Herron and Langway, 1980]. First the recently precipitated snow rearranges into a more compact position. Having reached the so called critical density of approximately $\rho_c = 550kg/m^3$ no further densification is obtainable through grain settling and the snow has been transformed to firn (the definitions of snow and firn are generally vague and somewhat overlapping). Thus entering the second stage interconnected air passages in the firn are slowly closed off. This process terminates at a density of $\sim 830kg/m^3$ where only air bobbles remain. At this density the firn has been transformed into ice. Finally in the third phase the air bobbles in the ice are compressed until the final density of $\rho_i = 917kg/m^3$ is reached.

In 1980 Herron and Langway presented an empirical model describing the first two stages of densification. Here a slightly modified version of their model will be used. The modifications were applied in order to better fit observed Greenland density profiles [Johnsen et al., 2000].
First of all the model assumes the following general relation between depth (z) and density (ρ):

$$\frac{d\rho}{dz} = K\rho(\rho_i - \rho) \qquad \rho_i = 917kg/m^3 \tag{3.3}$$

Where K may depend on temperature and accumulation rate at a given location. Using data from multiple polar ice cores Herron and Langway [1980] found empirical expressions for K. Hence for the first two stages of densification (3.3) can be written:

$$\frac{d\rho}{dz} = k_0\rho(\rho_i - \rho), \qquad \rho \leq \rho_c \tag{3.4}$$

$$\frac{d\rho}{dz} = k_1 c_w^{-0.5}\rho(\rho_i - \rho), \qquad \rho_c < \rho \leq \rho_{max} \tag{3.5}$$

Here c_w denotes the snow accumulation rate in meters of water equivalent, $\rho_c = 550kg/m^3$ is the critical density and $\rho_{max} = 800kg/m^3$ is the maximum density for which Herron and Langway [1980] found the model to be in agreement with observations. The values of k_0 and k_1 depends on the local temperature, T, (in kelvin):

$$k_0 = f_0 \cdot 0.011 \cdot e^{\frac{-0.106}{k_B T}} \tag{3.6}$$

$$k_1 = f_1 \cdot 0.575 \cdot e^{\frac{-0.223}{k_B T}} \tag{3.7}$$

Where $k_B = 8.6167 \cdot 10^{-5} ev/K$ is the Boltzmann constant and the two factors $f_0 = 0.85$ and $f_1 = 1.15$ are scaling constants introduced by Johnsen et al. [2000]. All other numerical constants in the above equations are determined by Herron and Langway [1980] as to bet fit observed density profiles from a variety of glaciers and ice sheets.
The density at a given depth (z) can also be derived from the model. For densities below ρ_c the following expression can be found by integration of (3.4):

$$\rho = \rho_i \frac{R_0 e^{\rho_i k_0 z}}{1 + R_0 e^{\rho_i k_0 z}}, \qquad R_0 = \frac{\rho_0}{\rho_i - \rho_0}, \qquad \rho \leq \rho_c \tag{3.8}$$

The density at the surface of the ice sheet given by ρ_0, which for central

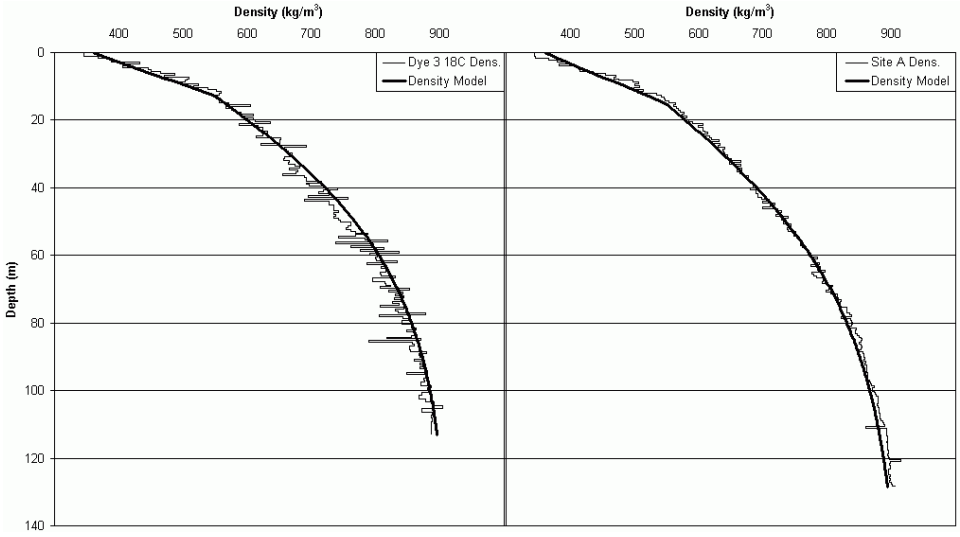

Figure 3.2: Measured and modelled density profiles for the southern Greenland Dye 3 18C ice core and the central Greenland Site A core. Temperature and accumulation data for the two drill sites have been used in the depth/density model.

Greenland conditions equals $\sim 360 kg/m^3$ [Johnsen et al., 2000].
The depth (z_c) at which $\rho = \rho_c$ can be found by rearrangement of (3.8):

$$z_c = \frac{ln(\rho_c/\rho_0)}{\rho_i k_0} \tag{3.9}$$

Integration of (3.5) leads to the depth/density relation for densities larger than ρ_c:

$$\rho = \rho_i \frac{R_c e^{\rho_i k_1 (z-z_c) c_w^{-0.5}}}{1 + R_c e^{\rho_i k_1 (z-z_c) c_w^{-0.5}}}, \qquad R_c = \frac{\rho_c}{\rho_i - \rho_c}, \qquad \rho > \rho_c \tag{3.10}$$

Finally it should be noted that (3.5) and (3.10) also are useable approximations for densities larger than ρ_{max} for central and southern Greenland conditions. This can be seen in figure 3.2. Hence the removal of the upper bound in (3.10).

3.2 Ice flow near an ice divide

Several attempts have been made to make simple models of flow in ice sheets [Haefeli, 1963; Nye, 1963; Dansgaard and Johnsen, 1969; Johnsen and Dansgaard, 1992 a]. All these models assumes two dimensional flow of

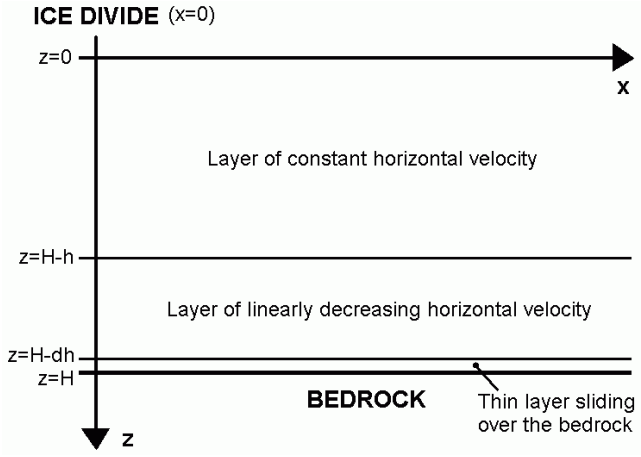

Figure 3.3: Schematic description of the ice flow model used for flow calculations near an ice divide.

an incompressible continuum of ice. The models are valid only close to the ridge of the ice sheet, i.e. nearby an ice divide.
The model which will be presented here relaxes the assumption of incompressibility. In the top of the ice sheet the flow model will instead assume that density obeys the Herron and Langway [1980] density model presented in the previous section.
Except for the relaxation of the incompressibility assumption, the new model is almost identical to the model presented by Johnsen and Dansgaard [1992 a]. Hence the model is designed to account for ice flow near an ice divide and is presented schematically in figure 3.3.

The model is based on the following assumptions:

- The flow is two dimensional.
- The thickness of the ice sheet (H) and the accumulation rate (c) are constant both in time and along the flow direction.
- The ice sheet is in a steady state.
- There is no melting at the bottom of the ice sheet.
- The horizontal velocity (u) in the ice sheet can be expressed as:

$$u = \begin{cases} U \cdot x & 0 \leq z \leq H - h \\ \left(1 - \frac{(z-H+h)(1-f_b)}{h-dh}\right) \cdot U \cdot x & H - h < z \leq H - dh \\ f_b U \cdot x & H - dh < z \leq H \end{cases} \qquad (3.11)$$

Here z is the depth, x is the distance from the ice divide and dh is

the thickness of a small layer of ice sliding over the bedrock. The ratio between the bottom sliding velocity and the surface velocity is given by f_b while U is a constant. The horizontal velocity is assumed independent of depth in the upper part of ice sheet. Below $z = H - h$ the velocity decreases linearly with depth until it reaches the bottom sliding velocity of $u = f_b U \cdot x$. Usually the model parameters h and f_b are determined from depth/age relations found in a given ice core. U will be derived later.

- The density varies only with depth and is given by:

$$\rho = \begin{cases} (3.8) \; and \; (3.10) & 0 \leq z \leq H - h \\ \rho_i & H - h < z \leq H \end{cases} \tag{3.12}$$

Where $\rho_i = 917 kg/m^3$ is the density of ice.
It should be noted that density in the Greenland ice sheet actually only increases in the upper ~200 meters while the depth of z=H-h typically is more than 1500 meters. The choice of z=H-h as the boundary of the layer with varying density is made only because it is practical not to introduce yet another boundary in the model. The density model (3.10) will yield almost constant densities ($\rho = \rho_i$) below the upper ~200 meters.

3.2.1 Assuring ice sheet mass balance

Using the steady state condition it is possible to derive the value of the constant U. Steady state implies that the ice accumulation must equal the horizontal mass transport:

$$c \cdot x = \int_0^H u \frac{\rho}{\rho_i} dz \tag{3.13}$$

Where c is the accumulation rate in meters of ice equivalent. Using (3.11) and (3.12) the above expression can be written:

$$\begin{aligned} c \cdot x &= \int_0^{H-h} Ux \frac{\rho}{\rho_i} dz + \int_{H-h}^{H-dh} \left(1 - \frac{(z - H + h)(1 - f_b)}{h - dh}\right) Ux dz \\ &+ \int_{H-dh}^{H} f_b U x dz \end{aligned} \tag{3.14}$$

Table 3.1: Flow parameters for different Greenland drill sites. For sources see the main text.

Drill site	H^*	h	dh	f_b	U	H_{eff}
	m	m	m		yr^{-1}	m
Crete	-	-	-	-	$1.23 \cdot 10^{-4}$	~ 2340
Dye 3	2013	300 ± 40	25	0.16	-	~ 1900
Milcent	2410	$0 - 330$	-	-	-	~ 2200
GRIP	3003.8	1200	6	0.15	-	~ 2500

Letting H^* be the ice thickness in meters of ice equivalent and z^* the depth in meters of ice equivalent (3.14) takes the form:

$$\begin{aligned} c &= \int_0^{H^*-h} U dz^* + \int_{H^*-h}^{H^*-dh} \left(1 - \frac{(z^* - H^* + h)(1-f_b)}{h - dh}\right) U dz^* \\ &+ \int_{H^*-dh}^{H^*} f_b U dz^* \end{aligned} \tag{3.15}$$

Carrying out the integrations and isolating U the following is obtained:

$$U = \frac{c}{H_{eff}}, \qquad H_{eff} = H^* - \frac{1}{2}(h + dh)(1 - f_b) \tag{3.16}$$

Where H_{eff} will be referred to as the effective ice thickness.
Flow model parameters for four different Greenland drill sites derived by Reeh et al. [1978], Hammer et al. [1978], Johnsen et al. [1992 a] and Dansgaard et al. [1993] as well as corresponding effective ice thicknesses are given in table 3.1. It should be noted that as the Milcent drill site is situated far from the central Greenland ice divide, this model can only be considered a crude approximation of the Milcent ice flow. Hence more sophisticated flow models have been developed for the Milcent drill site [Hammer et al., 1978]. In this survey however, the presented model assuming closeness to the ice divide will be used for the Milcent drill site, as this quite simple model does provide a reasonable approximation for the top few hundred meters of the ice sheet (the Milcent ice core only reaches a depth of 400m). Finally it will be assumed that the effective height at the Crete drill site can be used at the nearby Sites A to G (see table 2.1).

3.2.2 Expressions for the vertical strain rate

The vertical strain rate ($\dot{\varepsilon_z}$) can also be derived from the ice flow model. This is done by expressing $\dot{\varepsilon_z}$ in terms of the annual layer thickness (λ):

$$\dot{\varepsilon_z} = \frac{d\lambda}{\lambda dt} \tag{3.17}$$

Now the steady state condition implies that in one year, an annual layer of thickness λ is transported exactly the distance λ down through the ice sheet:

$$\lambda = w \cdot \tau, \qquad \tau = 1yr \tag{3.18}$$

Here $w = \frac{dz}{dt}$ is the vertical velocity in the ice sheet. Remembering that τ is just a constant (3.17) can be rewritten as:

$$\dot{\varepsilon_z} = \frac{dw}{wdt} = \frac{dw}{wdz}\frac{dz}{dt} = \frac{dw}{dz} \tag{3.19}$$

The steady state version of the continuity equation can then be used to evaluate $\frac{dw}{dz}$ for $z \leq H - h$:

$$\begin{aligned} \frac{d(\rho u)}{dx} + \frac{d(\rho w)}{dz} = 0 \Rightarrow \\ \rho\frac{du}{dx} + \rho\frac{dw}{dz} + w\frac{d\rho}{dz} = 0 \Rightarrow \\ \frac{dw}{dz} = -\frac{du}{dx} - w\frac{d\rho}{\rho dz} \end{aligned} \tag{3.20}$$

For $z > H - h$ the density is constant with depth and (3.20) reduces to:

$$\frac{dw}{dz} = -\frac{du}{dx} \tag{3.21}$$

Substituting (3.20) and (3.21) into (3.19) and using that $w = \frac{dz}{dt}$ the following expressions for the vertical strain rate are derived:

$$\dot{\varepsilon_z} = -\frac{du}{dx} - \frac{d\rho}{\rho dt} \qquad z \leq H - h \tag{3.22}$$

$$\dot{\varepsilon_z} = -\frac{du}{dx} \qquad z > H - h \tag{3.23}$$

The first term on the right hand side of (3.22) being due to flow related layer thinning, while the second term represents thinning due to densification.

3.2.3 Deriving the vertical velocity profile

Finally the vertical velocity (w) can be derived from (3.20) and (3.21). For $z \leq H - h$, w is found by solving the first order linear differential equation given by (3.20):

$$w(z) = e^{\int_0^z -\frac{d\rho}{\rho dz'}dz'} \left(\int_0^z \frac{du}{dx} \cdot e^{\int_0^{z'} \frac{d\rho}{\rho dz''}dz''} dz' + w_0 \right) \tag{3.24}$$

Where w_0 is the vertical velocity at the surface of the ice sheet. Defining ρ_0 as the density at the top of the ice sheet (3.24) can be rewritten as:

$$w(z) = e^{\int_{\rho_0}^{\rho} -dln\rho'} \left(\int_0^z \frac{du}{dx} \cdot e^{\int_{\rho_0}^{\rho'} dln\rho''} dz' + w_0 \right) \tag{3.25}$$

Now remembering that $u = U \cdot x$ for $z \leq H - h$ and using the depth/density relation (3.3):

$$w(\rho) = \frac{\rho_0}{\rho} \left(\int_{\rho_0}^{\rho} \frac{U}{K\rho_0(\rho_i - \rho')} d\rho' + w_0 \right) \tag{3.26}$$

For the steady state condition to be satisfied the vertical velocity at the surface of the ice sheet must equal $w_0 = \frac{\rho_i c}{\rho_0}$. Hence carrying out the integration in 3.26 the following is obtained:

$$w(\rho) = \frac{\rho_i c}{\rho} + \frac{U}{k_0 \rho} ln\left(\frac{\rho_i - \rho}{\rho_i - \rho_0}\right) \qquad \rho \leq \rho_c \tag{3.27}$$

$$w(\rho) = \frac{\rho_i c}{\rho} + \frac{U}{k_0 \rho} ln\left(\frac{\rho_i - \rho_c}{\rho_i - \rho_0}\right) + \frac{U c_w^{0.5}}{k_1 \rho} ln\left(\frac{\rho_i - \rho}{\rho_i - \rho_c}\right) \qquad \rho > \rho_c \tag{3.28}$$

Here it has been used that K has different values (see (3.4) and (3.5)) for densities smaller than and larger than $\rho_c = 550 kg/m^3$.
A profile of the vertical velocity in the ice sheet at the GRIP drill site is shown in figure 3.4. The profile was calculated using the above equations and the parameters given in tables (2.2) and (3.1). It can be seen that in the first tens of meters vertical velocity decreases rapidly as the snow and firn gets denser. Below some 200 meters where density is almost constant the decrease in velocity gets linear. Reassuringly this result is in complete agreement with results from the model of Johnsen and Dansgaard [1992 a] which assumes incompressibility of the ice.

Turning to the case where $z > H - h$, w can be found from (3.21). Using (3.11) two solutions have to be derived for different depth intervals:

$$w(z) = \int_{H-h}^{z} \left[\left(1 - \frac{(z' - H + h)(1 - f_b)}{h - dh} \right) \cdot U \right] dz' + w_{H-h} \tag{3.29}$$
$$for\ H - h < z \leq H - dh$$

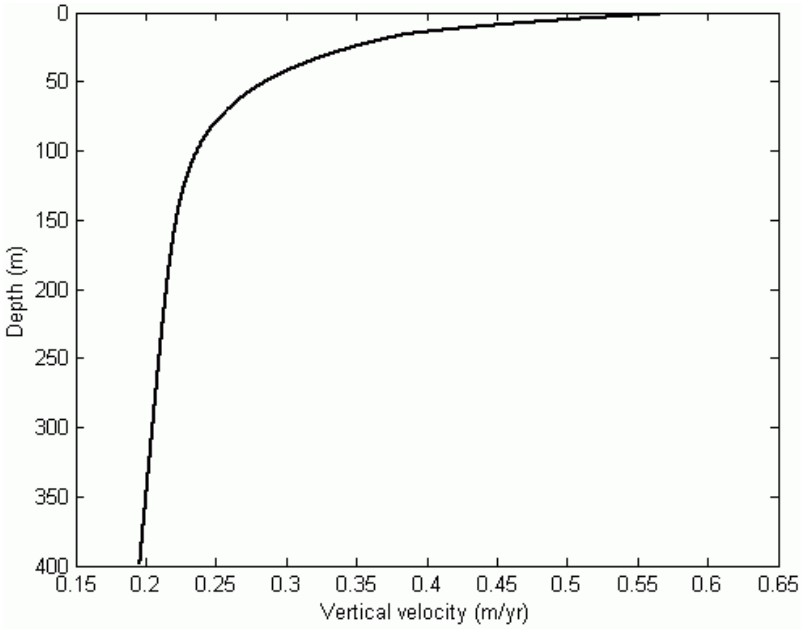

Figure 3.4: The vertical velocity profile at the GRIP drill site calculated for the top 400m of the ice sheet.

$$w(z) = \int_{H-dh}^{z} f_b U dz' + w_{H-dh}, \qquad H - dh < z \leq H \tag{3.30}$$

Where w_{H-h} can be found by substituting $\rho(z = H - h)$ into (3.28) and w_{H-dh} can be derived from (3.29). Carrying out the integrations in (3.29) and (3.30) the final expressions for w have the form:

$$w(z) = U\left[z - (H-h) - \frac{z(z-(H-h))(1-f_b)}{h-dh}\right] + w_{H-h} \tag{3.31}$$
$$for\ H - h < z \leq H - dh$$

$$w(z) = f_b U(z - (H - dh)) + w_{H-dh}, \quad H - dh < z \leq H \tag{3.32}$$

As density is assumed constant for $z > H - h$ the above equations yield the same vertical velocity profiles as the model presented by Johnsen and Dansgaard [1992 a].

3.3 The firn diffusivity

For densities larger than the effective pore close off density for diffusive processes ($\rho_{pc} = 804.3 kg/m^3$), diffusion through the interconnecting air passages in the firn becomes impossible. For densities smaller than ρ_{pc} [Johnsen et al., 2000] derived the following expression for the firn diffusivity:

$$\Omega = \gamma \left(1 - b\frac{\rho^2}{\rho_i^2}\right)\left(\frac{1}{\rho} - \frac{1}{\rho_i}\right) \qquad \rho \leq \rho_{pc} \tag{3.33}$$

Here $b = 1.3$ while γ depends on the stable isotope, temperature, pressure and some physical properties of water and ice:

$$\gamma = \frac{mp\Omega_a}{RT\alpha} \tag{3.34}$$

Where m is the molar weight of water, R is the gas constant, T the temperature in kelvin and p the saturation vapor pressure over ice (in Pa):

$$p = 3.454 \cdot 10^{12} \cdot e^{\frac{-6133}{T}} \tag{3.35}$$

The diffusivity of water vapor in air (Ω_a) is given by:

$$\Omega_a = \frac{2110}{q}\left(\frac{T}{T_0}\right)^{1.94}\left(\frac{P_0}{P}\right) \tag{3.36}$$

Here P is pressure in atm, $T_0 = 273.15K$ and $P_0 = 1atm$. The value of q depends on the stable isotope in question [Merlivat and Jouzel, 1979]:

$$q(O^{18}) = 1.0285 \quad and \quad q(D) = 1.0251 \tag{3.37}$$

The fractionation factor (α) is also dependent on the isotope:

$$\alpha(O^{18}) = 0.9722 \cdot e^{\frac{11839}{T}} \tag{3.38}$$

$$\alpha(D) = 0.9098 \cdot e^{\frac{16288}{T^2}} \tag{3.39}$$

3.4 Derivation of diffusion lengths

In sections 3.1 and 3.2 density and vertical velocity profiles as well as expressions for the vertical strain rate were obtained. The expression for the stable isotope diffusivity was outlined in the previous section. Hence enough information has been gathered to approach the main problem of deriving diffusion lengths for the stable isotopes down through the ice sheet.

3.4.1 Diffusion lengths in the snow and firn layers

The problem of deriving diffusion lengths down through the upper snow and firn layers of the ice sheet is a matter of solving the differential equation (3.2).
The differential equation can be integrated numerically to yield the diffusion lengths. It is however often more convenient to have approximative analytical solutions to the differential equation.
Hence Johnsen et al. [2000] found that it was possible to derive analytical solutions for the diffusion length (σ) from the differential equation (3.2) if a substitution from $\frac{d\sigma^2}{dt}$ to $\frac{d\sigma^2}{d\rho}$ was made and ice flow was disregarded in the calculation of $\dot{\varepsilon_z}$.
However, in order to obtain satisfying diffusion lengths Johnsen [pers. comm.] had to correct the obtained diffusion lengths for ice flow in a second stage of calculations.
Here a new approximative set of analytical solutions to equation (3.2) will be derived. As ice flow will be included in the derivation, no second stage correction will be needed for the obtained diffusion lengths.

First a substitution from $\frac{d\sigma^2}{dt}$ to $\frac{d\sigma^2}{d\rho}$ is made in equation (3.2):

$$\frac{d\sigma^2}{d\rho}\frac{d\rho}{dz}\frac{dz}{dt} = 2\dot{\varepsilon_z}\sigma^2 + 2\Omega \tag{3.40}$$

Now using that ($w = \frac{dz}{dt}$) and substituting the expression for $\dot{\varepsilon_z}$ (3.22), which includes ice flow into (3.40) the following is obtained:

$$\frac{d\sigma^2}{d\rho}\frac{d\rho}{dz}w = 2\left(-\frac{du}{dx} - w\frac{d\rho}{\rho dz}\right)\sigma^2 + 2\Omega \tag{3.41}$$

Acknowledging that for central Greenland conditions $\rho \leq \rho_{pc}$ has the consequence that the depth (z) automatically is (much) smaller than $H - h$ the following is obtained for firn diffusion:

$$\frac{d\sigma^2}{d\rho}K\rho(\rho_i - \rho)w = 2\left(-U - wK(\rho_i - \rho)\right)\sigma^2 + 2\Omega \qquad \rho \leq \rho_{pc} \tag{3.42}$$

Here the basic depth/density relation (3.3) has been used. Substituting the expressions for w when $z \leq H - h$ (3.27) and (3.28) into (3.42) yields:

$$\frac{d\sigma^2}{d\rho}\rho(A + B) = -2\left(A + B + C\right)\sigma^2 + 2\Omega \qquad \rho \leq \rho_{pc} \tag{3.43}$$

Where A, B and C are given by:

$$A = \begin{cases} k_0 c \frac{\rho_i}{\rho}(\rho_i - \rho) & \rho \leq \rho_c \\ k_1 c_w^{-0.5} c \frac{\rho_i}{\rho}(\rho_i - \rho) & \rho > \rho_c \end{cases} \tag{3.44}$$

$$B = \begin{cases} \frac{U}{\rho}(\rho_i - \rho) ln\left(\frac{\rho_i - \rho}{\rho_i - \rho_0}\right) & \rho \leq \rho_c \\ \frac{U}{\rho}(\rho_i - \rho)\left(\frac{k_1}{c_w^{0.5} k_0} ln\left(\frac{\rho_i - \rho_c}{\rho_i - \rho_0}\right) + ln\left(\frac{\rho_i - \rho}{\rho_i - \rho_c}\right)\right) & \rho > \rho_c \end{cases} \tag{3.45}$$

$$C = U = \frac{c}{H_{eff}} \tag{3.46}$$

As solving the differential equation (3.43) is very complicated, a scale analysis of the terms A, B and C is performed. Using typical central Greenland values of $c = 0.25m/year$, $H_{eff} = 2500m$, $T = 243K$ and $\rho_0 = 360kg/m^3$ the following is obtained for $\rho_0 \leq \rho \leq \rho_{pc}$:

$$max\left(\left|\frac{B}{A}\right|\right) \sim 2 \cdot 10^{-2} \quad and \quad max\left(\left|\frac{C}{A}\right|\right) \sim 1 \cdot 10^{-1} \tag{3.47}$$

Hence neglecting ice flow completely and only retaining the term A, an error of $\sim 10\%$ must be expected. If both the terms A and C are retained however, the expected error drops to $\sim 2\%$. It is therefore decided to neglect only the complicated B term, retaining the ice flow information given by the C term.
Substituting the expression for firn diffusivity (3.33) into (3.43) and retaining the A and C terms only, the following is obtained:

$$\frac{d\sigma^2}{d\rho} = -2\sigma^2\left(\frac{1}{H_{eff} K \rho_i(\rho_i - \rho)} + \frac{1}{\rho}\right) + \frac{2\gamma}{Kc\rho\rho_i^2}\left(1 - b\frac{\rho^2}{\rho_i^2}\right) \tag{3.48}$$

$$for\ \rho_0 \leq \rho \leq \rho_c :\ K = k_0 \quad and \quad for\ \rho_c < \rho \leq \rho_{pc} :\ K = k_1 c_w^{-0.5}$$

Assuming isothermal firn layers, this is a first order linear differential equation with the following solution:

$$\sigma^2 = e^{-\int_{\rho_n}^{\rho} 2\left(\frac{1}{H_{eff} K \rho_i(\rho_i - \rho')} + \frac{1}{\rho'}\right) d\rho'} \left(\int_{\rho_n}^{\rho} \frac{2\gamma}{Kc\rho'\rho_i^2}\left(1 - b\frac{\rho'^2}{\rho_i^2}\right) \cdot e^{\int_{\rho_n}^{\rho'} 2\left(\frac{1}{H_{eff} K \rho_i(\rho_i - \rho'')} + \frac{1}{\rho''}\right) d\rho''} d\rho' + \sigma_n^2\right) \Rightarrow \tag{3.49}$$

$$\sigma^2 = \left(\frac{\rho_n}{\rho}\right)^2 \left(\frac{\rho_i - \rho}{\rho_i - \rho_n}\right)^{\kappa} \left(\frac{2\gamma}{Kc\rho_n^2\rho_i^2} \int_{\rho_n}^{\rho} \left(\frac{\rho_i - \rho_n}{\rho_i - \rho'}\right)^{\kappa} \left(\rho' - b\frac{\rho'^3}{\rho_i^2}\right) d\rho' + \sigma_n^2\right) \tag{3.50}$$

Where K is given by (3.48) and κ, ρ_n and σ_n are defined in the following manner:

$$\rho_n = \begin{cases} \rho_0 & for \quad \rho_0 \leq \rho \leq \rho_c \\ \rho_c & for \quad \rho_c < \rho \leq \rho_{pc} \end{cases} \tag{3.51}$$

$$\sigma_n = \begin{cases} \sigma_0 = 0 & for \quad \rho_0 \leq \rho \leq \rho_c \\ \sigma_c = \sigma(\rho_c) & for \quad \rho_c < \rho \leq \rho_{pc} \end{cases} \tag{3.52}$$

$$\kappa = \frac{2}{\rho_i H_{eff} K} \tag{3.53}$$

Now, the integration on the right hand side of (3.50) can be parted in two:

$$\sigma^2 = \left(\frac{\rho_n}{\rho}\right)^2 \left(\frac{\rho_i - \rho}{\rho_i - \rho_n}\right)^\kappa \left(\frac{2\gamma}{Kc\rho_n^2\rho_i^2}\left(I - \frac{b}{\rho_i^2}II\right) + \sigma_n^2\right) \tag{3.54}$$

Where I and II are the two integrals:

$$I = \int_{\rho_n}^{\rho} \rho' \left(\frac{\rho_i - \rho_n}{\rho_i - \rho'}\right)^\kappa d\rho' \quad and \quad II = \int_{\rho_n}^{\rho} \rho'^3 \left(\frac{\rho_i - \rho_n}{\rho_i - \rho'}\right)^\kappa d\rho' \tag{3.55}$$

Using integration by parts the value of these integrals can be obtained:

$$\int \rho^p \left(\frac{\rho_i - \rho_n}{\rho_i - \rho}\right)^\kappa d\rho = \rho^p \left(\tfrac{\rho_i-\rho_n}{\rho_i-\rho}\right)^{\kappa-1} \left(\tfrac{\rho_i-\rho_n}{\kappa-1}\right) - \int p \cdot \rho^{p-1} \left(\tfrac{\rho_i-\rho_n}{\rho_i-\rho}\right)^{\kappa-1} \left(\tfrac{\rho_i-\rho_n}{\kappa-1}\right) d\rho \quad \kappa \neq 1 \tag{3.56}$$

For central Greenland conditions $\kappa \ll 1$. Applying (3.56) one and three times to the integrals I and II respectively, yields the following results:

$$I = \left(\tfrac{\rho_i-\rho_n}{\kappa-1}\right) \left[\rho \left(\tfrac{\rho_i-\rho_n}{\rho_i-\rho}\right)^{\kappa-1} - \rho_n - \left(\tfrac{\rho_i-\rho_n}{\kappa-2}\right) \left(\left(\tfrac{\rho_i-\rho_n}{\rho_i-\rho}\right)^{\kappa-2} - 1\right)\right] \tag{3.57}$$

$$II = \left(\tfrac{\rho_i-\rho_n}{\kappa-1}\right) \left\{\rho^3 \left(\tfrac{\rho_i-\rho_n}{\rho_i-\rho}\right)^{\kappa-1} - \rho_n^3 - 3\left(\tfrac{\rho_i-\rho_n}{\kappa-2}\right) \left[\rho^2 \left(\tfrac{\rho_i-\rho_n}{\rho_i-\rho}\right)^{\kappa-2} - \rho_n^2 - 2\left(\tfrac{\rho_i-\rho_n}{\kappa-3}\right) \left\langle \rho \left(\tfrac{\rho_i-\rho_n}{\rho_i-\rho}\right)^{\kappa-3} - \rho_n - \left(\tfrac{\rho_i-\rho_n}{\kappa-4}\right) \left[\left(\tfrac{\rho_i-\rho_n}{\rho_i-\rho}\right)^{\kappa-4} - 1\right] \right\rangle \right] \right\} \tag{3.58}$$

Hence substituting (3.57) and (3.58) into (3.54) and using the definitions

provided by (3.51), (3.52) and (3.53), diffusion lengths can be calculated for $\rho_0 \leq \rho \leq \rho_{pc}$. As the densities as a function of depth are given by (3.8) and (3.10), it is possible to obtain diffusion lengths for $0 \leq z \leq z_{pc}$. Here z_{pc} is the depth that corresponds to the density ρ_{pc}.
The obtained diffusion lengths for the GRIP drill site are presented in figure 3.5 (red curve). Also shown in the figure are the diffusion lengths which would be found if only the term A was retained in equation (3.43) (green curve). The blue curve in the figure shows diffusion lengths calculated through numerical integration of equation (3.43) with all the terms A, B and C included.
From figure 3.5 it can be seen that when both the A and C terms are retained in equation (3.43) the analytical solutions are very close to the numerically derived solutions. When only the A term is retained and ice flow therefore is disregarded, the analytical solutions deviates much more from the numerical integration. The lack of ability to account for flow related thinning of the snow and firn layers is seen to lead to a clear overestimation of the diffusion lengths. A second stage flow correction is therefore clearly needed in order to bring the green curve in agreement with the numerically calculated blue curve.

In contrast the analytically derived diffusion lengths, which were found solving equation (3.43) with both the term A and the term C retained, never

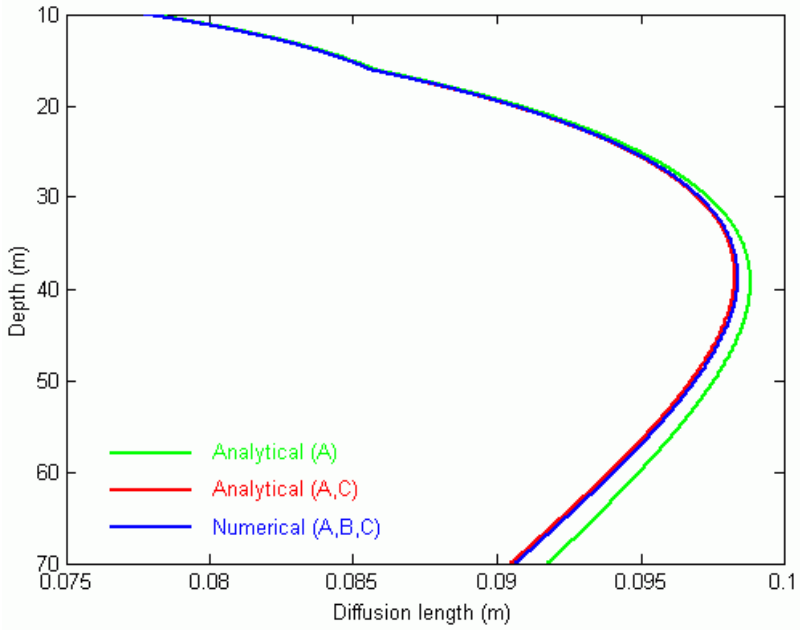

Figure 3.5: Diffusion lengths calculated for the GRIP drill site using different types of analytical approximated solutions to equation 3.43 or numerical integration of the equation.

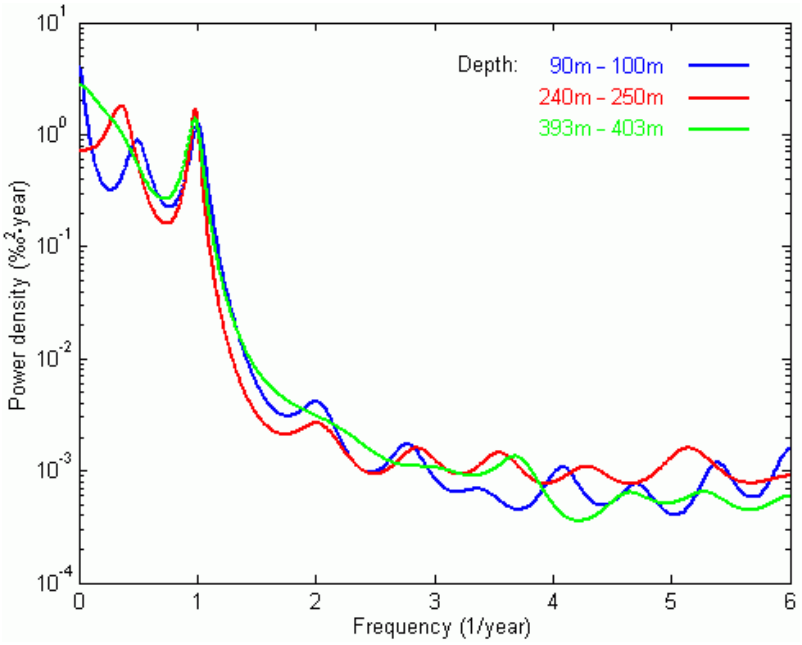

Figure 3.6: MEM spectral densities (m=20) for different depth intervals of the detailed Crete ice core $\delta^{18}O$ profile.

deviates more than 0.2% from the numerically calculated diffusion lengths. It is therefore feasible to use the presented analytical expressions for the diffusion lengths without any second stage correction.

3.4.2 Diffusion lengths in the ice

Turning to depths bellow z_{pc}, the dominant diffusion process is expected to be single ice crystal self diffusion. Detailed analysis of Greenland ice core data does however find that other more effective diffusive processes must play a role at least below ~500m [Johnsen et al. 2000]. This so called "excess diffusion" is not well understood, but known to have a diffusivity two to three orders of magnitude smaller than the typical firn diffusivity [Johnsen et al. 2000]. Hence the following analysis will be based on the assumption that no diffusion takes place below the depth of pore close off. This assumption is supported by the MEM power spectra presented in figure 3.6 (for details on the maximum entropy method, MEM, see appendix D). The spectra showing no significant dampening of the annual cycle below 90 meters depth (the depth of z_{pc} is approximately 70 meters). In fact analytical integration of the annual spectral peaks (using a method developed in [Johnsen and Andersen, 1978]) gives the powers $0.45‰^2$, $0.39‰^2$ and $0.48‰^2$ for the intervals $90m - 100m$, $240m - 250m$ and $393m - 403m$ respectively.

Neglecting diffusion implies that (3.40) can be reduced to the following

expression:

$$\frac{d\sigma^2}{dz}\frac{dz}{dt} = 2\dot{\varepsilon}_z\sigma^2 \qquad z > z_{pc} \tag{3.59}$$

Using (3.19) this can be rewritten as:

$$\frac{d\sigma^2}{dz}w = 2\frac{dw}{dz}\sigma^2 \qquad z > z_{pc} \tag{3.60}$$

This reduces to a simple differential equation which is directly solvable through separation of variables:

$$\int_{\sigma_{pc}^2}^{\sigma^2}\frac{d(\sigma^2)'}{(\sigma^2)'} = 2\int_{z_{pc}}^{z}\frac{dw}{wdz'}dz' = 2\int_{w_{pc}}^{w}\frac{dw'}{w'} \qquad z > z_{pc} \tag{3.61}$$

Here σ_{pc} and w_{pc} represents the diffusion length and vertical velocity at depth z_{pc}. Carrying out the integrations leads to the following solution:

$$\sigma = \sigma_{pc}\frac{w}{w_{pc}} \qquad w < w_{pc} \tag{3.62}$$

Hence calculating w from (3.27), (3.28) and (3.31), diffusion lengths for depths below z_{pc} can be found. For depths below $\sim 500m$ this formula probably predicts too small diffusion lengths as the "excess diffusion" was not included in the derivation.
It should also be noted that the formula is completely invalid for depths below ~1600m, as ice below this depth originates from precipitation during the last glaciation and the accumulation rates over Greenland were greatly reduced during that time period.

Diffusion lengths calculated for the GRIP ice core (drilled at the summit of the Greenland ice sheet) are presented in figure 3.7. A clear difference between deuterium and ^{18}O is observed due to a higher deuterium fractionation factor (α) and hence a lower deuterium diffusivity.
It is also possible to express the diffusion lengths in terms of the the annual layer thickness in the ice sheet (see figure 3.8). In this manner it can easily be seen that the only reason for the decrease of the diffusion lengths below z_{pc} (~70m) shown in figure 3.7 is the layer thinning. Hence when expressed in terms of layer thickness the diffusion lengths are seen to remain constant below z_{pc} in figure 3.8).
Diffusion lengths in figure 3.8) shows a steady increase only as long as diffusive processes take place.

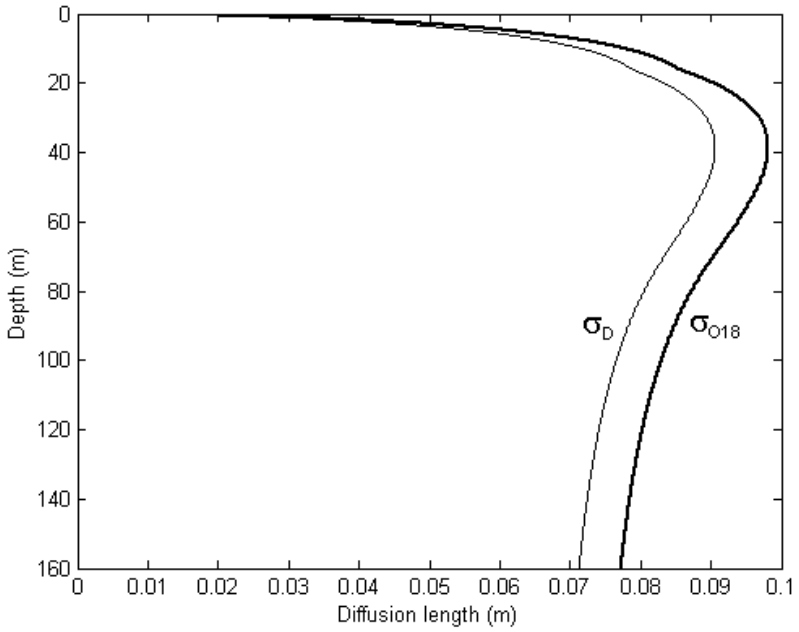

Figure 3.7: Stable isotope diffusion lengths versus depth for the GRIP ice core.

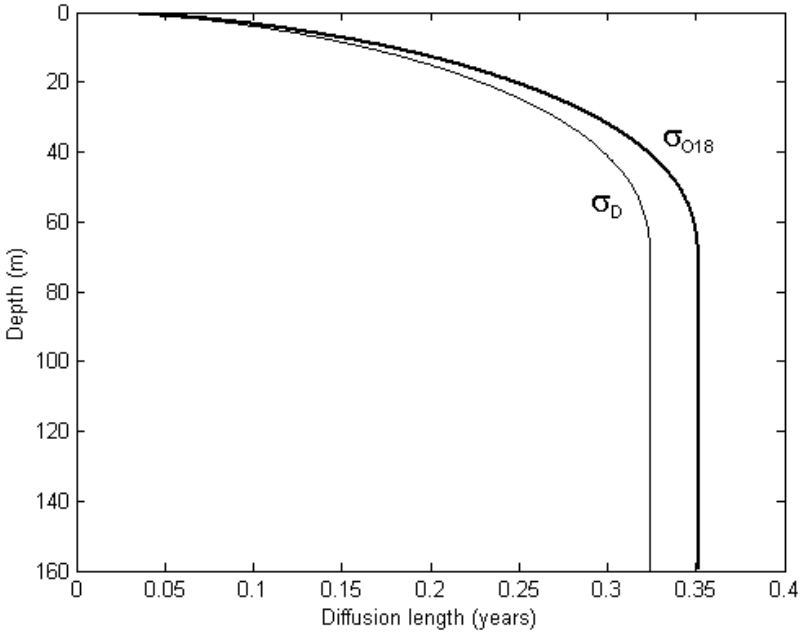

Figure 3.8: As in figure 3.7 except the diffusion lengths now are shown in fractions of the thickness of a annual layer in the GRIP ice core.

3.5 Summary

Using a slightly modified version of the densification model presented by Herron and Langway [1980] a simple two dimensional ice flow model including densification was presented.
This flow model and a model for the diffusivity of stable isotopes in snow and firn presented by Johnsen et al. [2000] gave the foundation for the calculation of diffusion lengths.
A scale analysis of the governing differential equation for the diffusion lengths led to a simplification of the equation.
Analytical expressions for the diffusion lengths which satisfied the simplified differential equation were derived.
The derived diffusion lengths were found to be an excellent approximation to diffusion lengths obtained through numerical integration of the complete differential equation.
For depths below the effective pore close off density, diffusion lengths were found assuming that diffusive processes ceases.

Chapter 4

Retrieving Seasonal Ice Core Stable Isotope Data

The process of obtaining seasonal time scale information from the highly resolved series of measured ice core stable isotope data is quite extensive. A number of calculational choices and compromises have to be made in this process.
Such decisions concerning the practical steps in the calculations can be of immense importance. Hence this chapter will thoroughly formulate and document the calculational approach used for retrieving the seasonal stable isotope data.

4.1 Diffusion correction of stable isotope data

Having derived formulas for diffusion length in the previous chapter it is possible to mathematically reconstruct seasonal variations using (3.1). The basic idea being to transform data into Fourier components and then use (3.1) to correct the amplitude of each Fourier component for diffusive dampening.
The following formulation of this technique will lend from the mathematics of fourier transformation of continuous periodic functions. A reformulation is however needed in order to transform the discrete stable isotope data.
As papers on diffusion correction generally provide very few details concerning this practical part of the correction process, this derivation has been carried out independently.
Having a subset of $2N+1$equally spaced stable isotope data, the amplitudes of the corresponding Fourier components can be derived as follows:

$$A_k = \frac{\Delta x}{L} \sum_{i=-N}^{N} \delta_i \cdot C_k^i, \quad C_k^i = \frac{1}{\Delta x} \int_{(i-\frac{1}{2})\Delta x}^{(i+\frac{1}{2})\Delta x} cos(kx)dx \tag{4.1}$$

$$B_k = \frac{\Delta x}{L} \sum_{i=-N}^{N} \delta_i \cdot S_k^i, \quad S_k^i = \frac{1}{\Delta x} \int_{(i-\frac{1}{2})\Delta x}^{(i+\frac{1}{2})\Delta x} sin(kx)dx \tag{4.2}$$

Where A_k and B_k are the amplitudes of Fourier cosine and sine components of wave numbers k while δ_i is a given data value, Δx is data spacing and $2L = (2N+1)\Delta x$ is the total length of the data set.
Hereafter the data set can be approximated by its truncated Fourier series:

$$\delta(x) \simeq \bar{\delta} + \sum_{k=1}^{K} (A_k cos(kx) + B_k sin(kx)) \tag{4.3}$$

Where K is the maximum wave number and $\bar{\delta}$ is the data mean.
Focusing on the central value (δ_0) it is possible to rewrite 4.3:

$$\delta_0 \simeq \frac{1}{\Delta x} \int_{-\frac{\Delta x}{2}}^{\frac{\Delta x}{2}} \delta(x)dx = \frac{1}{\Delta x} \int_{-\frac{\Delta x}{2}}^{\frac{\Delta x}{2}} \left(\bar{\delta} + \sum_{k=1}^{K} A_k cos(kx) \right) dx \Rightarrow$$

$$\delta_0 \simeq \bar{\delta} + \sum_{k=1}^{K} A_k C_k^0, \qquad C_k^0 = \frac{1}{\Delta x} \int_{-\frac{\Delta x}{2}}^{\frac{\Delta x}{2}} cos(kx)dx \tag{4.4}$$

Here it has been used that the sine function vanishes because it is an odd function ($sin(-x) = -sin(x)$). Recalling (3.1) it is possible to obtain the diffusion corrected value (δ_0^{dc})for the single measurement δ_0:

$$\delta_0^{dc} \simeq \bar{\delta} + \sum_{k=1}^{K} A_k C_k^0 e^{\frac{1}{2}k^2\sigma^2} \tag{4.5}$$

Using (4.1) this can be rewritten in terms of the original data set:

$$\delta_0^{dc} \simeq \bar{\delta} + \sum_{k=1}^{K} \left(\frac{\Delta x}{L} \sum_{i=-N}^{N} \delta_i \cdot C_k^i \right) C_k^0 e^{\frac{1}{2}k^2\sigma^2} \tag{4.6}$$

An expression which can be rewritten changing the order of summation:

$$\delta_0^{dc} \simeq \bar{\delta} + \tfrac{\Delta x}{L} \textstyle\sum_{i=-N}^{N} \delta_i \left(\sum_{k=1}^{K} C_k^i C_k^0 e^{\frac{1}{2}k^2\sigma^2} \right) \Rightarrow$$

$$\delta_0^{dc} \simeq \bar{\delta} + \tfrac{\Delta x}{L} \textstyle\sum_{i=-N}^{N} \delta_i f_i(K,\sigma), \quad f_i(K,\sigma) = \sum_{k=1}^{K} C_k^i C_k^0 e^{\frac{1}{2}k^2\sigma^2} \tag{4.7}$$

Hence for a given choice of wave number cutoff (K) a set of filter coefficients (f_i) can be derived when the diffusion length (σ) is known. Applying the filter to the $2N+1$ data values it is possible to corrected the central value (δ_0) for diffusion.

When diffusion correcting an entire stable isotope data series from an ice core, the filter length $(2N+1)$ is usually much smaller than the total number of ice core data. Hence the method presented in (4.7) can be used for most of the data. The method does however not immediately apply to the first N data at the top and the last N data at the bottom of the ice core. This is of course due to the fact that the method only corrects the central value for diffusion, but uses the $2N$ adjacent values in the process.
In order to use the filter method all the way to the very top and bottom of the ice core, the data are therefore artificially extended with N values at the top and the bottom of the core. This is done using MEM prediction [Andersen, 1974] (see appendix D for more on MEM), which assures that the extended series has the same spectral properties as the original series.

4.1.1 Choosing wave number cutoff and filter length

When choosing the filter length two factors have to be considered. First, a long filter improves the ability of the Fourier components to resolve the data. Second, the method implicitly assumes that the diffusion length remains constant for the entire filter length. An assumption which is violated more and more as filter length increases.
A thorough analysis of this problem will not be performed here, but it was found that a filter length of 100-200 seemed to balance the two demands.
The wave number cutoff K has to be selected carefully to assure that annual oscillations are retained, while noise in the data is not amplified to an extend where it destroys the climatic signal.
High frequency oscillations are attenuated the most by diffusive dampening. Hence such oscillations will also be amplified the most in the process of diffusion correction. Noise in the high frequency spectrum will therefore be amplified greatly by the diffusion correction.
In order to avoid having the diffusion corrected data seriously contaminated by noise, K was chosen as low as was possible when the annual oscillations had to be resolved. This was done by constraining the filter to only resolve frequencies, which had to be amplified less than a fixed maximum amplification (Amp_{max}):

$$e^{\frac{1}{2}k^2\sigma^2} \leq Amp_{max} \tag{4.8}$$

Using more than 1400 years of accumulation data from the Crete ice core the standard deviation of annual accumulation was determined to be 19%. In order to resolve years with very little accumulation, Amp_{max} was chosen to always accommodate oscillations of a length down to 62% of the mean annual accumulation. This was however not feasible for the Site E, Site G and GRIP cores (the cores with the lowest accumulation rates) as the noise level raised quickly for $Amp_{max} > 70$ (see figure 4.1).

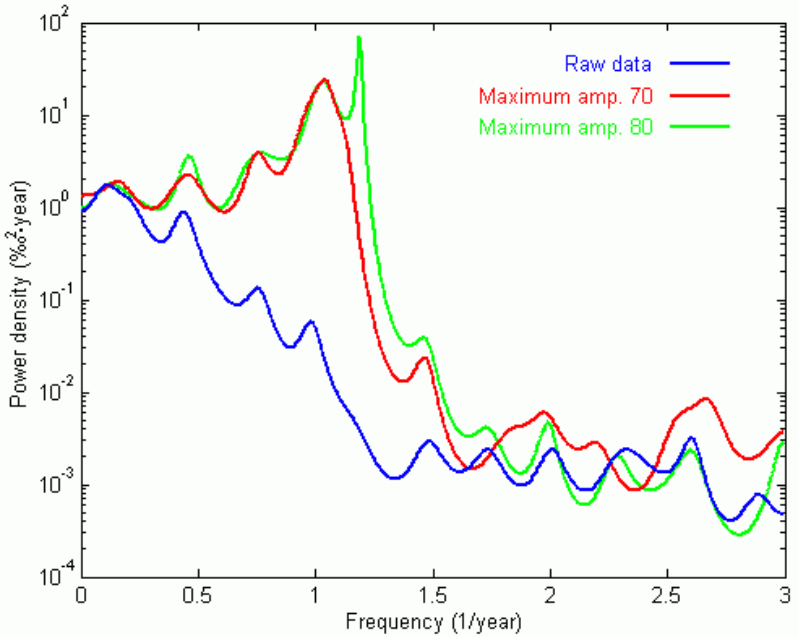

Figure 4.1: MEM spectral densities (m=30) for raw $\delta^{18}O$ data and diffusion corrected $\delta^{18}O$ data with two different amplitude cutoffs. Data are from the bottom 20m of the Site E ice core.

The choices of Amp_{max} for the different ice cores are shown in table 4.1. The table does not provide any information on the Dye 3 drill site as diffusion correction is not possible at this southern location due to melt layers in the ice cores. The melt layers impede diffusion and seriously distort any attempt to diffusion correct the data.
Table 4.1 also gives the data spacing (Δx). It should be noted that some of the ice cores are sampled according to a cutting scale. Samples in those cores span the same fraction of a year but differ in length. This is however not a problem since Δx can be a spacing both in time step and depth; the only demand being equal spacing.

4.1.2 Analysis of the annual cycles

If seasonal climatic signals are to be extracted, it is of great importance that the annual cycle in the stable isotope data is preserved. A dampening or amplification of the annual cycle would unavoidably lead to a false trend in seasonal data. Hence having diffusion corrected the ice core data using the information provided by tables 2.2, 3.1 and 4.1, it was decided to examine the stability of the annual cycle in the corrected data. The ice cores from the Sites A-G, Crete and Milcent are very diverse in accumulation rates

Table 4.1: Filter parameters used for diffusion correction.

Drill site	N	Amp_{max}	Δx
Crete	50	50	0.083yr
Milcent	50	5	0.129yr
Site A	50	60	0.123yr
Site B	50	40	0.118yr
Site D	50	20	0.101yr
Site E	50	70	0.167yr
Site G	50	70	0.149yr
GRIP	100	70	0.025m

(table 2.2) and hence very diverse in choice of filter parameters (table 4.1). Therefore diffusion corrected data from these cores were chosen for further investigation.
Using the same technique to evaluate the power of the annual cycle as in section 3.4.2, different intervals in the ice cores were examined (see table 4.2. All peaks in the power spectrum at frequencies between $0.75yr^{-1}$ and $1.25yr^{-1}$ were regarded as being part of the annual cycle.
It is very satisfactory that the values given in table 4.2 only shows small and unsystematic fluctuations in the power of the annual cycle. The values are also in broad agreement with a annual cycle power estimate of $7 - 12‰^2$ obtained from snow pits at the same drill sites also using MEM power estimation (the snow pit data being only slightly affected by diffusion).

With respect to the Dye 3 site, the initial estimate made in the Vinther et al. [2003 a] paper (appendix A) was that because of high accumulation rates in southern Greenland, seasonal data from the Dye 3 ice cores could

Table 4.2: Power of the annual cycle for different data intervals in the ice cores after correction for diffusion. All values are found using MEM power estimation with m=40 and are given in $‰^2$.

	Data intervals (Sample number)				
Drill site	1-700	701-1400	1401-2100	2101-2800	2801-6300
Crete	7.1	7.9	9.1	8.9	7.2
Milcent	6.7	8.0	7.0	7.0	7.1
Site A	7.9	6.9	6.3	7.3	-
Site B	8.1	9.2	7.3	-	-
Site D	9.0	7.9	9.7	-	-
Site E	11.3	11.1	-	-	-
Site G	8.8	8.2	-	-	-

Table 4.3: Power of the annual cycle for different data intervals in two Dye 3 ice cores, which have not been corrected for diffusion. All values are found using MEM power estimation with m=40 and are given in $‰^2$.

	Data intervals (Sample number)			
Drill site	1-400	401-800	801-1200	1201-8300
Dye 3 79	2.5	2.3	1.5	1.7
Dye 3 18C	2.4	1.5	1.3	-

be used without diffusion correction.
It was decided to test this assertion by investigating the power of the annual cycle in the raw $\delta^{18}O$ data in two Dye 3 ice cores. The natural choice being the deepest core (Dye 3 79) and the core with least accumulation (Dye 3 18C).
Table 4.3 shows that the annual cycle in the Dye 3 cores is in fact damped by diffusion, despite the high accumulation rates at the drill sites. Assuming the annual cycles to be harmonic oscillations, their amplitudes are proportional to the square root of the power given in table 4.3. Thus amplitudes of the annual cycles in the Dye 3 ice cores are reduced to 75-80% from their values in the top ~40m (corresponding to the top 400 measurements). The final dampening of the annual cycle seems to be almost equal for the two Dye 3 sites (79 and 18C). Below the depth of effective pore close off (70m ~ sample number 800) where diffusive processes become much less important, the amplitude of the annual cycle stabilizes in the Dye 3 79 (deep) core.
Thus having demonstrated that annual cycles in the Dye 3 ice cores are indeed influenced by diffusion it could seem natural to focus on other Greenland ice cores only (as diffusion correction is impossible due to melt layers). This would however have the consequence that no ice core data from southern Greenland were available for seasonal interpretation.

Being confronted with the grim choice of either leaving out a significant amount of climatic information from southern Greenland, or alternatively introduce known non-climatic trends into the seasonal data following the approach in the Vinther et al. [2003 a] paper, it was decided to once again turn to diffusion correction.
Melt layers in the Dye 3 cores tend to create sharp gradients in the stable isotope signal, which in turn results in noisy large amplitude oscillations when data are diffusion corrected. Even though melt layers are formed only in very warm summers at the Dye 3 site, the few melt layers present are enough to seriously distort the diffusion corrected data. Hence it was clear that a new approach was needed.
It was therefore decided to apply the diffusion correction to the data, but this time in reverse. Hence the part of the stable isotope data obtained at depths above the depth of effective pore close off, where artificially diffused.

Table 4.4: Power of the annual cycle for different data intervals in two Dye 3 ice cores, which have been artificially diffused. All values are found using MEM power estimation with m=40 and are given in $‰^2$.

	Data intervals (Sample number)			
Drill site	1-400	401-800	801-1200	1201-8300
Dye 3 79	1.4	2.1	1.5	1.7
Dye 3 18C	1.1	1.3	1.3	-

To obtain a stable annual cycle these data were diffused exactly as much as nature would have diffused them (according to the model), had they reached the depth of pore close off or below where diffusive processes ceases (see figure 3.8).
The powers of the annual cycles at different data intervals after artificial diffusion, are given in table 4.4, again focusing on the Dye 3 79 and Dye 3 18C cores.
Table 4.4 clearly suggests that that the artificial diffusion removes the trends in the amplitudes of the annual cycles. Hence it was decided to use the artificially diffused data for further investigation.
With respect to the calculation details of the artificial diffusion the following should be mentioned: As the artificial diffusion dampens the fourier components no high frequency cutoff was needed; the high frequency noise no longer being amplified. The cutoff was now solely decided by the maximum frequency resolvable by the data. The filter parameters used for all Dye 3 cores were ($N = 100, \Delta x = 0.125$) except for Dye 3 18C where ($\Delta x = 0.152$). The Dye 3 effective height given in table 3.1 was used for all cores. Meteorological data were provided by table 2.2 and temperature at the Dye 3 4B site was assumed equal to the temperature observed at the nearby Dye 3 71/79 drill site. The temperature at the Dye 3 18C site was assumed to be one degree below the Dye 3 71/79 site, due to the altitude difference of 130m.
Finally it could be asked why artificial diffusion was not chosen as the preferred diffusion correction method, when noise amplification problems are avoided using this method. Here one should however remember that artificial diffusion in fact mixes the summer and winter stable isotope signal. It can only be applied to the Dye 3 ice core data because of the high accumulation rate at the Dye 3 drill site. There the relatively small mixing of the seasons is a tolerable price to pay for a stable signal. The diffusional mixing of seasons has nothing to do with the original climatic signal recorded in the stable isotopes. Hence it must always be the main goal to reconstruct the original climatically related stable isotope signal despite the problems of noise amplification.

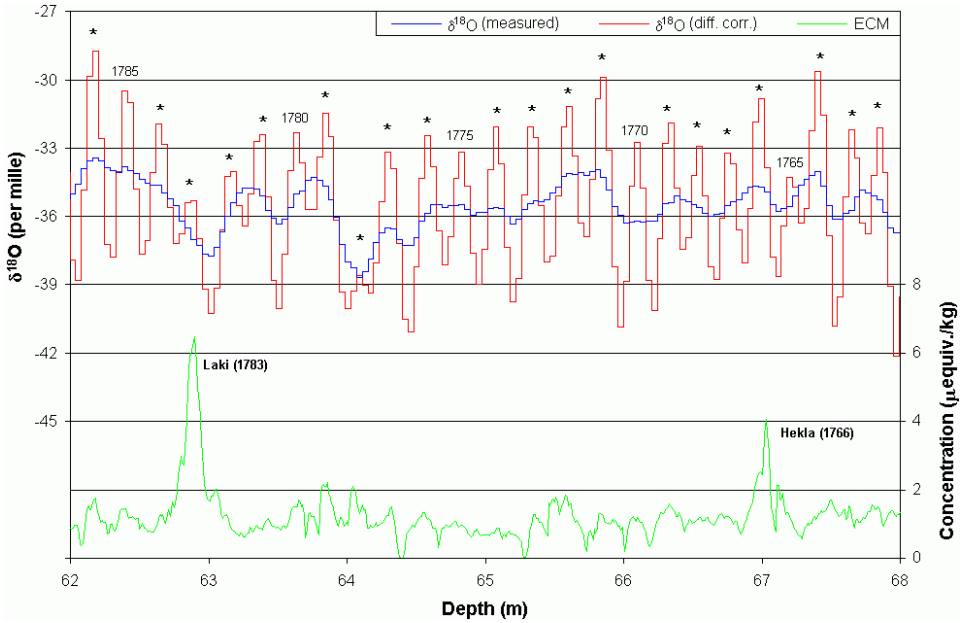

Figure 4.2: Interval of the Site E ice core illustrating the dating of the core. The dating is mainly done by counting of the annual $\delta^{18}O$ cycles in the diffusion corrected data. Volcanic reference horizons in the ECM signal are used for guidance.

4.2 Dating the ice cores

Before further analysis of the seasonal data is possible a careful dating of the ice cores have to be carried out. The dating is mainly done by counting the annual cycles in the $\delta^{18}O$ data. For the high accumulation sites (Dye 3 and Milcent) the counting can be carried out on the raw measured data. In ice cores from drill sites of more modest accumulation it is necessary to use the diffusion corrected data for the counting (see figure 4.2).
In this survey dating was carried out on the diffusion corrected (or artificially diffused) data for all ice cores for consistency. All ice cores are dated in corporation with Henrik Clausen from the glaciology group at NBIfAFG. Fixed reference horizons are an important verification tool in the dating process. In figure 4.2 it can be seen how known volcanic eruptions can be detected in Electric Conductivity Measurements (ECM) data and used for dating. Summer melt layers are another example of reference horizons used for the dating.
When multiple cores are available it is also very helpful to compare characteristic features in the $\delta^{18}O$ data.

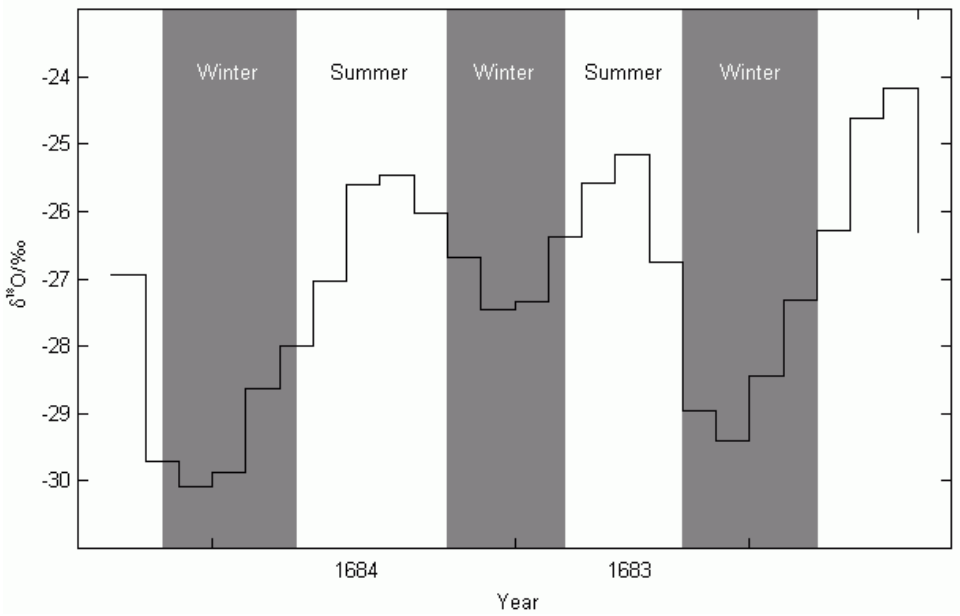

Figure 4.3: Example from the Dye 3 79 ice core demonstrating the selection of winter and summer season stable isotope data. Note the consistently high $\delta^{18}O$ values during the winter 1683/84. During this particular winter, it is known that a so called frost fair (a marked) was held on the frozen river Thames in London. Hence this winter is a clear example of an NAO signal in the stable isotope data.

4.3 Extraction of seasonal variations

To extract the seasonal signals from the stable isotope data it is necessary to pinpoint summers and winters in the data. It was decided to define midwinters and midsummers as respectively the minima and maxima of the annual cycle in the stable isotopes. The winter season was then defined as half the values between the adjacent midsummers and vice versa for summers (see figure 4.3). Hence the average of one half of the annual data is calculated for the winter season data while the average of the other half is calculated for the summer season data.
In the Vinther et al. [2003 a] paper a somewhat smaller amount of data was used for the winter season analysis (appoximately 30% of the annual data), but here the 50% are chosen in order to maximize data use and hence minimize the noise in the seasonal data.

4.4 The noise level in the seasonal data

When multiple ice core records from the same drill site are available, it is possible to obtain information about the noise level in the data. Johnsen et al. [1997] presented a formula for the signal to noise variance ratio, but gave no derivation of the expression. Here the Johnsen et al. [1997] formula will be derived.
This analysis assumes that N ice core data series (δ_i) each containing a signal (s_i) and a noise component (n_i) are available:

$$\begin{aligned} \delta_1 &= s_1 + n_1 \\ \delta_2 &= s_2 + n_2 \\ &\cdot \\ &\cdot \\ \delta_N &= s_N + n_N \end{aligned} \tag{4.9}$$

As the cores are from the same drill site, they are assumed to contain the same signal (s):

$$s = s_1 = s_2 = ... = s_N \tag{4.10}$$

The noise in each ice core record is assumed to be independent, random and white, but to have the same variance:

$$var(n_1) = var(n_2) = ... = var(n_N) \tag{4.11}$$

As the signal is the same in all the cores, the signal variances are also identical:

$$var(s_1) = var(s_2) = ... = var(s_N) \tag{4.12}$$

Assuming that signal and noise are uncorrelated in the ice core records, the following relation holds:

$$var(\delta_i) = var(s_i) + var(n_i) \tag{4.13}$$

Defining the mean noise and signal variances of the cores as:

$$var_n = \frac{1}{N}\sum_{i=1}^{N} var(n_i) \qquad var_s = \frac{1}{N}\sum_{i=1}^{N} var(s_i) \tag{4.14}$$

Then the following expression for the mean ice core data variance var_δ can be obtained (using (4.13)):

$$var_\delta = \frac{1}{N}\sum_{i=1}^{N} var(\delta_i) = \frac{1}{N}\sum_{i=1}^{N}(var(s_i) + var(n_i)) = var_s + var_n \quad (4.15)$$

Now using the N records it is possible to form a stacked ice core record (δ_S):

$$\delta_S = \frac{1}{N}\sum_{i=1}^{N}\delta_i \quad (4.16)$$

As the signals in all the records are the same, while the noise in each record is independent, then the variance of the stacked record is given by:

$$var(\delta_S) = var_s + \frac{1}{N}var_n \quad (4.17)$$

Using (4.15) and (4.17) it is possible to obtain the following expression of the single ice core signal to noise variance ratio:

$$S/N = \frac{var_s}{var_n} = \frac{var(\delta_S) - \frac{1}{N}var_\delta}{var_\delta - var(\delta_S)} \quad (4.18)$$

Which is identical to the expression for S/N given in Johnsen et al. [1997] (except for a printing error in that paper, which causes the S/N to be negative).
It can be seen from (4.17) that the effect of stacking N ice core records, will be to increase the signal to noise ratio N times.

Signal to noise variance ratios determined for summer and winter data from the Dye 3 and GRIP drill sites are given in table 4.5. Ice cores should be no more than ~2km apart, if they are to be expected to contain the same

Table 4.5: Signal to noise variance ratios in the seasonal $\delta^{18}O$ data for ice cores from the Dye 3 and GRIP drill sites.

Drill site	Sum. (S/N)	Win. (S/N)	Years used[a]	Ice cores used
Dye 3	1.73	1.56	1239-1970	71, 79[b]
GRIP	0.70	0.51	1728-1974	89-1, 89-3, 91, 92, 93

[a]The maximum number of years common to all cores were used.
[b]The Dye 3 18C and 4B cores were left out as they are situated more than 2km from the other two Dye 3 cores.

signal [Fisher et al., 1996]. Hence it was not possible to calculate signal to noise ratios for the Milcent, Crete and Site A-G cores as there is only one core at each site.
At the Dye 3 drill site S/N is almost three times higher than at the GRIP site for both summer and winter data. This difference is a clear consequence of the much higher accumulation rate at Dye 3 (see table 2.2). The seasons in the GRIP cores are just barely resolved and the stacking of three GRIP cores is needed to obtain the same S/N as in one Dye 3 core.
Summer season data are seen to have a higher S/N than winter season data. This is most probably a consequence of the winters having more severe (windy) conditions than the summers.
It should be mentioned that the GRIP S/N ratios obtained here are somewhat smaller than the the S/N of 0.87-0.97 found from almost the same cores by Johnsen et al. [1997]. This is however to be expected because annual data was used by Johnsen et al. [1997]. The seasonal data are only based on half of the annual data and are therefore more affected by noise.
Likewise the S/N of $\sim$2.4 found by Fisher et al. [1985] for annually resolved Dye 3 data is somewhat larger than the S/N ratios obtained here for seasonal Dye 3 data.

4.5 Retrieving regional climatic signals

Having obtained multiple stacked or unstacked records of seasonal $\delta^{18}O$ it is desirable to reduce complexity in the data set. This can be done using a variety of empirical orthorgonal function (EOF) techniques. All such EOF methods aim at isolating common patterns of variability in the data.
Applying various EOF techniques to ice core data is indeed very useful in isolating regional climatic signals in the $\delta^{18}O$ [Fisher et al., 1996, Rogers et al., 1997, Vinther et al., 2003 a].
The specific EOF method, called principal component analysis (PCA) has become widely used in various projects aimed at reconstructing past climate variability [Jones, 1987; Jones et al., 1999, Luterbacher et al., 2002]. Hence it was decided to apply PCA to the seasonal ice core $\delta^{18}O$ data.
The following presentation of the concept of PCA, is largely drawn from the analysis of Cook et al. [1994].
It is assumed that N ice core based time series (δ_i) of seasonal $\delta^{18}O$ each of length M are ready for analysis. Further it is assumed that M>N, which is always the case in this survey.
The first step is to form the covariance matrix (C) for the N data series:

$$C = \begin{pmatrix} cov(\delta_1,\delta_1) & cov(\delta_1,\delta_2) & \dots & cov(\delta_1,\delta_N) \\ cov(\delta_2,\delta_1) & cov(\delta_2,\delta_2) & \dots & cov(\delta_2,\delta_N) \\ \vdots & \vdots & \ddots & \vdots \\ cov(\delta_N,\delta_1) & cov(\delta_N,\delta_2) & \dots & cov(\delta_N,\delta_N) \end{pmatrix} \tag{4.19}$$

All the elements in the diagonal of C will equal 1.
Hereafter the eigenstructure of C is determined from the equation:

$$det|C - \beta I| = 0, \quad \beta = (\beta_1, \beta_2, \ldots \beta_N) \tag{4.20}$$

Where I is the N dimensional identity matrix.
Solution of (4.20) yields the N eigenvalues, β_1 to β_N. They are commonly arranged in descending order, i.e. $\beta_1 > \beta_2 > \ldots > \beta_N$.
Each eigenvalue has a corresponding eigenvector of length N. These eigenvectors are called principal components in the PCA terminology:

$$PC1 = \begin{pmatrix} PC1_1 \\ PC1_2 \\ \vdots \\ PC1_N \end{pmatrix}, \ \ldots, \ PCN = \begin{pmatrix} PCN_1 \\ PCN_2 \\ \vdots \\ PCN_N \end{pmatrix} \tag{4.21}$$

Hence β_1 corresponds to $PC1$, β_2 corresponds to $PC2$ et cetera.
The principal components are vectors with different weights on each of the ice cores, $PC1_1$ being the weight of the first principal component ($PC1$) on the first ice core (δ_1), $PC1_2$ being the weight of $PC1$ on the second ice core (δ_2) and so on.
The N principal components are all orthogonal to each other and form a new basis for the data set (the old basis being the N individual ice cores).
Just as each of the ice cores has a corresponding time series of length M, so has each of the principal components:

$$PC1_t = \sum_{i=1}^{N} PC1_i \delta_i, \ldots, \ PCN_t = \sum_{i=1}^{N} PCN_i \delta_i \tag{4.22}$$

Where $PC1_t$ is the time series corresponding to the $PC1$, $PC2_t$ is the time series corresponding to the $PC2$ and so on.
Importantly, the size of each eigenvalue corresponds to how much of the total data set variance each principal component explains:

$$PC1(var.\ exp.) = \beta_1 / \sum_{i=1}^{N} \beta_i, \ldots, \ PCN(var.\ exp.) = \beta_N / \sum_{i=1}^{N} \beta_i \tag{4.23}$$

Hence from the PCA a set of ice core structures (the principal components) can be obtained. Each structure explaining a known amount of variance in the ice core data. As the eigenvalues were sorted in descending order, the $PC1$ will have the largest eigenvalue and therefore explain the largest amount of data set variance. The PCN in contrary will explain only a very

little amount of the total data variance.
The PCA can therefore provide valuable information on common patterns of variability in the ice core data, with the $PC1$ being the most important such pattern.

Chapter 5

Seasonal $\delta^{18}O$ as a Proxy for Seasonal Temperatures

As $\delta^{18}O$ first and foremost is known as a proxy for temperature, it is natural to make a comparison between seasonal $\delta^{18}O$ and seasonal temperatures from the Greenland area. In this manner the ability of the seasonal $\delta^{18}O$ data to capture the regional temperature variations can be assessed.
In order to increase the signal to noise ratio in the seasonal ice core data, ice core records were stacked before comparison with the seasonal temperature data whenever possible. Hence the four ice core records from the Dye 3 area were stacked as well as the five GRIP cores. The single core from the Milcent drill site was not stacked with any other ice core records.
Climatic conditions are known to change as one passes the central Greenland ice divide. The divide is situated in a north-south direction and passes through the GRIP and Crete drill sites and between the sites A and B. Stacking of all the records from the sites A to G and Crete would eliminate any differences in the cores related to the ice divide. It was therefore decided to stack the eastern ice cores from the sites A, E and G into one record (Crete (E)) and the sites B, D and Crete into a another central/western record (Crete (C/W)), see figure 5.1.

5.1 Greenland and Iceland temperature data

Most of the Greenland temperature observation sites have been in operation for the past few decades only [Cappelen et al., 2001] and are therefore not suitable for comparison with the ice core data (most ice cores in this survey were drilled some twenty years ago). Luckily, a few meteorological observation stations have records reaching back into the 19th century [Frich et al, 1996]. Some of these records do unfortunately have gaps in their observation series, while other series are from various sources [Hann et al., 1890; Frich et al, 1996; Peterson et al., 1997; Cappelen et al., 2001; Jørgensen, 2001] and

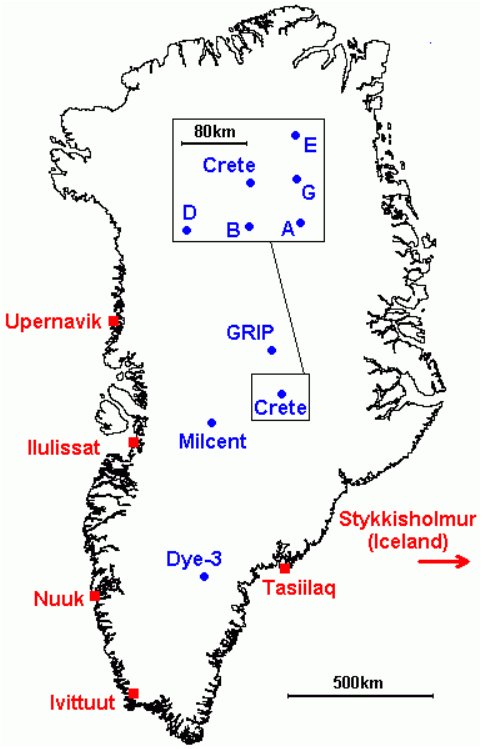

Figure 5.1: Locations of temperature observation stations (red) as well as ice core drill sites (blue).

were in need of some homogenization. Details of the homogenization of the series and the infilling of missing values using observations from neighboring stations, are given in appendix B.
As the south and west coast were the first parts of Greenland to be colonized, four out of five of the long Greenland temperature records are from these areas (see table 5.1 and figure 5.1). The single east coast record begins as late as 1894 A.D.
East and west coast Greenland climates are known to be very different indeed, and it is therefore unfortunate only to have one single and relatively short series of east coast observations available for comparison with the ice core data. Hence it was decided to also use temperature observations from the Iceland meteorological station at Stykkisholmur for the comparison. As Stykkisholmur has an impressive series of observations [Jonsson, 1989] and is situated only a few hundred kilometers from the Greenland east coast, it is an almost ideal substitute for an east coast station.
Table 5.1 provides details concerning all the temperature stations for which observations have been used in this survey.

Table 5.1: Temperature observation site details.[a]

Observation site	Lat. °N	Long. °W	Elevation m a.s.l.	First year	Missing seasons[b] Winter/Summer
Upernavik	72.78	56.17	122	1873	1/0
Ilulissat	69.22	51.05	39	1840	6/6[c]
Nuuk	64.17	51.75	50	1866	1/0[c]
Ivittuut	61.20	48.20	30	1873	3/4[c]
Tasiilaq	65.60	37.63	52	1894	1/4
Stykkisholmur	65.08	22.73	8	1823[d]	0/0

[a]Data sources are: [Hann, 1890; Frich et al., 1996; Jonsson, 1989, Cappelen et al., 2001].
[b]Only seasons until 1970 are counted.
[c]Some months are infilled using nearby stations - see appendix B.
[d]All months from 1823 to 1845 are based on adjusted Reykjavik observations.

5.2 The winter season

The four winter season stacked ice core records from Crete (C/W), Crete (E) Dye 3 and GRIP as well as the single Milcent record were compared to the Nov-Apr temperature observations available from the Greenland and Stykkisholmur meteorological stations. As the seasonal ice core data are based on 50% of the annual data, it was deemed reasonable to use 50% of the annual temperature observations as well. This decision relies on the observation (table 13.1 in Cappelen et al. [2001]) that Greenland precipitation is approximately equally distributed over the year when disregarding a tendency for more winter precipitation on the Greenland east coast and more summer precipitation on the west coast. Unfortunately no reliable precipitation measurements exist for the Greenland ice sheet itself.
Correlations between winter season ice core data and Nov-Apr temperature data are given in table 5.2.

From table 5.2 it can be seen that the Crete (E) record is mostly associated with Greenland east coast winter temperatures while the Crete (C/W) record is most significantly correlated to the southern and western Greenland stations. This difference supports the idea of dividing the Crete area ice cores into two different stacks. It should be noted, that quite surprisingly the Crete (C/W) record is the ice core record most strongly associated to the Icelandic (Stykkisholmur) winter temperature, suggesting that the Crete (E) record is capturing a somewhat local temperature signal also recorded at Tasiilaq.
Both the stacked Dye 3 record and the single Milcent record are strongly associated with southern and western Greenland winter temperatures while only containing little information about Greenland east coast and Icelandic

Table 5.2: Correlations[a] between winter season $\delta^{18}O$ and Nov-Apr temperature observations[b] for 4 different stacked and one single ice core record(s).

Drill site Temp. site	Crete (C/W)	Crete (E)	Dye 3	GRIP	Milcent
Upernavik	0.49	0.45	0.43	0.38	0.45
Ilulissat	0.55	0.41	0.57	0.44	0.46
Nuuk	0.55	0.46	0.61	0.43	0.55
Ivittuut	0.56	0.48	0.66	0.41	0.58
Tasiilaq	0.46	0.57	0.35	0.41	0.37
Stykkisholmur	0.44	0.37	0.23	0.30	0.33

[a]All correlations are significant above the 95% level.
[b]All available seasons of observation are used for each temp. station.

Table 5.3: Correlations between winter season $\delta^{18}O$ and Nov-Apr temperature observations[b] for the GRIP ice core records.

Drill site Temp. site	89-1	89-3	91	92	93
Upernavik	0.33	0.10[a]	0.35	0.28	0.24
Ilulissat	0.30	0.18	0.37	0.36	0.28
Nuuk	0.39	0.11[a]	0.35	0.36	0.26
Ivittuut	0.34	0.15[a]	0.38	0.31	0.28
Tasiilaq	0.31	0.11[a]	0.37	0.24	0.39
Stykkisholmur	0.14[a]	0.19	0.29	0.18	0.24

[a]Correlations that are not significant at the 95% level.
[b]All available seasons of observation are used for each temp. station.

winter temperatures.
The GRIP ice core stack is not associated with any particular Greenland region and seems to be quite weakly related to the Greenland winter temperatures. Even though this central Greenland site was found to have a low data signal to noise ratio, it is surprising that so little seasonal climatic information can be recovered despite the use of five ice core records in the GRIP stack. Hence an investigation into the causes of the weak relation between the GRIP stack and temperature will be performed.
Table 5.3 gives the correlations between each GRIP ice core record and the coastal Greenland and Iceland temperatures. It is immediately seen that one record in particular (GRIP 89-3) relates very weakly to the temperature records. In fact the GRIP 89-3 record is insignificantly correlated to 4 out of 5 Greenland Nov-Apr temperature records.

This result is in agreement with White et al. [1997], who for annually resolved GRIP ice core data also found that the GRIP 89-3 data had much weaker relations with Greenland annual temperatures than al other GRIP records.
White et al. [1997] tried to find a reason for this surprising result, but were unable to do so. No problems specific to the GRIP 89-3 data could be found in this survey either.
Having no reason to specifically disregard the GRIP 89-3 ice core record, one must accept that cores drilled at the GRIP site cannot always be expected to have significant relations with Greenland coastal temperatures.
Following the approach used in the Vinther et al. [2003 a] paper (appendix A) it was decided to use principal component analysis (PCA) in order to isolate regional scale signals from the seasonal Greenland ice core records. In order not to introduce a local climatic bias into the PCA it was decided to use the stacked ice core records in the PCA analysis; assuring equal weight for the different drill sites despite the different numbers of ice cores. Finally it was decided not to include the GRIP data in the PCA. The relations between GRIP data and seasonal temperatures were deemed to be too unreliable, given the results from the GRIP 89-3 record. If included in the PCA the GRIP stack was found to generally degrade the climatic signals isolated by the PCA.

The PCA was carried out for the maximum number of winter seasons common to all the ice cores, i.e. for the period 1778-1970. Referring to the terminology developed in section 4.5, N=4 ice core records all containing the same M=193 winter seasons were used.
The weights on the Crete (C/W), Crete (E), Dye 3 and Milcent records when forming the principal components are given in table 5.4. The table also shows the variance explained by each component.
The first principal component (PC1) is composed of almost equal parts of all the ice core records. As the PC1 also explains an impressive 62% of the variance in the four ice core records, it represents a clear regional signal present in all the ice cores.

Table 5.4: Ice core weights on the principal components for the winter season.

	PC1	PC2	PC3	PC4
Crete (C/W)	0.54	-0.17	-0.26	-0.78
Crete (E)	0.50	-0.56	-0.33	0.57
Dye 3	0.50	-0.01	0.86	0.06
Milcent	0.46	0.81	-0.27	0.23
Var. exp.	62%	16%	13%	9%

Table 5.5: Correlations[a] between the time series of the 4 winter season principal components and Nov-Apr temperature observations[b]

Component Temp. site	$PC1_t$	$PC2_t$	$PC3_t$	$PC4_t$
Upernavik	0.57	0.01	-0.09	0.06
Ilulissat	0.62	0.05	0.10	-0.11
Nuuk	0.68	0.08	0.06	0.02
Ivittuut	0.70	0.08	0.07	0.06
Tasiilaq	0.54	-0.22	-0.19	0.22
Stykkisholmur	0.43	-0.03	-0.21	-0.06

[a]All correlations larger than 0.23 are significant above the 95% level.
[b]All available seasons of observation are used for each temp. station.

The PC1 explained variance found in the Vinther et al. [2003 a] paper (see table A.2 in appendix A) is much smaller, this is probably an effect of the smaller number of ice cores stacked in the paper. Stacking less cores results in a smaller S/N ratio. Hence a weaker climatic signal will be common to all the records. This will decrease the record covariance and thereby the explained variance of the PC1.
Due to the low explained variances of the PC2, PC3 and PC4 it is difficult to interpret their climatic relevance. It should be noted though, that since the PC2 has strong weight, but of opposite sign on the Crete (E) and Milcent ice core records it probably reflects the east/west difference observed in Greenland climate.
Correlations between the time series of the principal components and Nov-Apr temperature observations are given in table 5.5. Almost all information in the winter season ice core records on Greenland winter temperature conditions seems to be extracted by the $PC1_t$. It has almost 50% of its variance in common with the southern and western Greenland stations of Ivittuut and Nuuk (the correlation squared gives the variance). Simultaneously it shares almost 30% of its variance with the east Greenland station of Tasiilaq. If the three temperature records from Ivittuut, Nuuk and Tasiilaq are stacked, the correlation with the $PC1_t$ increases to 0.76 suggesting that nearly 60% of the variance in the $PC1_t$ is related to a combination of southern Greenland east and west coast winter temperatures. This result being almost identical to the findings in the Vinther et al. [2003 a] paper, who found 56% variance in common between the winter season ice core $PC1_t$ and southern Greenland Dec-Mar temperatures (see table A.3 in appendix A).
Turning to the other principal components only very weak relations to Greenland temperatures can be found. The $PC2_t$ showing a weak tendency to have some east/west differences in correlation sign.

5.3 The summer season

Using the same approach as with the winter season ice core $\delta^{18}O$ data, summer season ice core data were compared to May-Oct temperature observations in the Greenland area (see table 5.6).
Associations between south-western Greenland summer temperatures and summer season $\delta^{18}O$ data are seen to be much weaker than is the case for the winter season. It should however be noted that Greenland temperature variations are 2-3 times stronger during winter times than during summer times. Hence the summer temperature signal is much weaker than the winter signal and therefore harder to capture.
Correlations between the Greenland east coast station (Tasiilaq) and the ice cores are only slightly smaller in summer than in winter. Relations between temperatures at this station and the ice core $\delta^{18}O$ data seem to be almost unaffected by the summer to winter variability drop.
Remarkably relationships between Icelandic summer temperatures and the ice core summer data are slightly strengthened as compared to the winter season. This despite a 50% winter to summer temperature variability drop at Stykkisholmur.
All the ice core records except the westernmost from the Milcent drill site, are in fact most significantly correlated to Tasiilaq and Stykkisholmur summer temperatures.

To further investigate the summer $\delta^{18}O$ data it was decided once again to use PCA on the ice core records. To facilitate comparison with the winter season PCA, it was decided to use exactly the same approach as before. In doing so, the GRIP data were again excluded.
The weights on the Crete (C/W), Crete (E), Dye 3 and Milcent records when forming the principal components are provided by table 5.7. The table also gives the variance explained by each component.

Table 5.6: Correlations[a] between summer season $\delta^{18}O$ and May-Oct temperature observations[b] for 4 different stacked and one single ice core record(s).

Drill site Temp. site	Crete (C/W)	Crete (E)	Dye 3	GRIP	Milcent
Upernavik	0.24	0.04	0.20	0.14	0.21
Ilulissat	0.22	0.03	0.29	0.19	0.26
Nuuk	0.33	0.05	0.37	0.20	0.38
Ivittuut	0.31	0.00	0.35	0.19	0.43
Tasiilaq	0.42	0.19	0.44	0.37	0.34
Stykkisholmur	0.38	0.37	0.47	0.37	0.21

[a]All correlations larger than 0.23 are significant above the 95% level.
[b]All available seasons of observation are used for each temp. station.

Table 5.7: Ice core weights on the principal components for the summer season.

	PC1	PC2	PC3	PC4
Crete (C/W)	0.58	-0.02	0.34	-0.74
Crete (E)	0.51	-0.57	0.32	0.56
Dye 3	0.46	-0.11	-0.88	-0.03
Milcent	0.43	0.81	0.11	0.37
Var. exp.	52%	21%	18%	10%

Just as was the case for the winter data, there is a regional scale PC1 with almost equal weights on all ice core records. This regional signal explains 52% of the variance in the ice core records. The $PC1_t$ has almost 25% of its variance in common with the Tasiilaq and Stykkisholmur summer temperature records (see table 5.8). The associations between the PC1 and Greenland west coast temperatures are generally weak.
The PC2 has almost the same east/west structure in summer and in winter. The summer PC2 does however explain a bit more of the ice core variance. The $PC2_t$ is significantly (but still weakly) correlated to southwestern Greenland temperature observations (see table 5.8). The $PC3_t$ and $PC4_t$ are not significantly correlated to any of the temperature observations and their climatic relevance is probably minor.

Table 5.8: Correlations[a] between the time series of the 4 summer season principal components and May-Oct temperature observations[b]

Component Temp. site	$PC1_t$	$PC2_t$	$PC3_t$	$PC4_t$
Upernavik	0.23	0.14	-0.07	-0.11
Ilulissat	0.27	0.18	-0.18	-0.08
Nuuk	0.37	0.27	-0.18	-0.11
Ivittuut	0.36	0.36	-0.18	-0.10
Tasiilaq	0.48	0.16	-0.13	-0.09
Stykkisholmur	0.49	-0.10	-0.18	-0.02

[a]All correlations larger than 0.23 are significant above the 95% level.
[b]All available seasons of observation are used for each temp. station.

5.4 Summary

Through a combination of ice core stacking and PCA, seasonal climatic information was retrieved from the seasonal ice core $\delta^{18}O$ data.
The $PC1_t$ of winter season $\delta^{18}O$ was found to be strongly associated with temperature conditions at the Greenland southern and western coastal areas. Traces of the difference in east and west coast Greenland winter temperatures were found in the $PC2_t$.
The $PC1_t$ of summer season $\delta^{18}O$ was found to be associated with Greenland east coast as well as Icelandic summer temperatures. The summer $PC2_t$ was related to Greenland south-west coast temperatures. Further the summer PC2 was found to be almost identical to the winter PC2 in its structure.

Chapter 6

Seasonal $\delta^{18}O$ and North Atlantic Region Atmospheric Flow Patterns and Sea Surface Temperatures

Significant relations between the seasonal $\delta^{18}O$ data and seasonal Greenland and Iceland temperatures were found in the previous chapter. Greenland temperatures are influenced both by atmospheric flow and the sea surface temperatures (SST) and sea ice conditions of the surrounding waters. It is therefore reasonable to expect the seasonal stable isotope data to be associated with both flow patterns and SST. This chapter is devoted to bring forward such associations.

As almost all the information of climatic relevance seems to be present in the ice core $PC1_t$ and $PC2_t$, these time series will be investigated further in this chapter.

Ideally a comparison between the ice core data and atmospheric flow in the 700hPa layer (the pressure layer where the drill sites are situated) should be made. Time series of observations of northern hemisphere 700hPa flow are however not very long. In fact only some 20 years of data are available for comparison with the ice core data, because the ice core data terminates as early as 1970.

It was therefore decided to compare the ice core data to the much larger database of north Atlantic region sea level pressure (SLP) observations. Making it possible to establish relations over a period of almost a 100 years.

6.1 The sea level pressure data

In order to obtain a clear picture of the north Atlantic region flow patterns associated with the seasonal ice core $\delta^{18}O$ variability it is preferable to use grided SLP data.
The northern hemisphere (NH) 5 ° latitude by 10 ° longitude monthly mean SLP data set from the Climate Research Unit (CRU), Norwich, UK spans the time period from 1873 to present [Jones, 1987]. As this is one of the most widely used and longest SLP datasets available, it was chosen for this investigation.
The CRU data set does only have true NH coverage for the period 1941-1970. This is due to a significant lack of pressure observations over large parts of Asia and the Pacific for the years before 1941. Fortunately observations in the Atlantic and European area provides enough information for the SLP data set to have coverage in the north Atlantic region, all the way back to 1873.

6.2 The sea surface temperature data

During the past decades a large effort have been made to build up the International Comprehensive Ocean-Atmosphere Data Set (I-COADS) [Slutz et al., 1985; Elms; 1993; Woodruff, 2001].
As part of the effort, two 2 ° latitude by 2 ° longitude monthly mean SST data sets have been generated. One set uses only ship based SST measurements and has somewhat stricter criteria for homogeneity than the other data set, that uses several kinds of SST observations (such as drifting and moored buoys).
Since homogeneity is essential when trying to establish solid climatic relations, it was decided to use the data set consisting only of ship based SST observations.
This SST data set covers the period 1800-1997. Here only the 20th century data will be used, as the 19th century data only covers the main shipping routes, which are situated away from Greenland waters.

6.3 Obtaining spatial response patterns to winter season $\delta^{18}O$ variability

For each year Nov-Apr averages were derived from the CRU monthly pressure data set. Subsequently the averages were used to obtain spatial responses of SLP to a 1σ change in the $PC1_t$ (and $PC2_t$). The responses were calculated by means of linearly regressing the SLP time series for each grid point separately against the $PC1_t$ ($PC2_t$). The slopes obtained from the linear regressions where thereafter used for the plot.
As with the SLP data Nov-Apr averages were calculated for each year in the

SST data set. It was however not possible to use the above regression technique to obtain the spatial SST response patterns as well. The SST data set has a considerable amount of missing values. It was therefore necessary to accept that each grid point regression were carried out for differing numbers observation years.
Carrying out the regression in this manner is somewhat unsatisfactory as grid points are no longer directly comparable. Some grid points may have data from periods with large SST variations, which could yield large regression coefficients, while other grid points had data from periods with smaller SST variations, maybe yielding smaller regression coefficients.
To counter such differences originating from data availability, it was decided to calculate correlation coefficients for each grid point instead of the linear regressions used for the SLP data. Further only grid points with less than 60% missing values were used for the calculation.
It should be stressed however, that even these measures are insufficient to assure direct comparability between grid points. Hence only patterns of SST variability in the correlation plots, which will be presented are of significance, not single grid point results.

6.4 The winter season

In figure 6.1 the period 1874-1970 (year of January) of the pressure data was used for regression. The SLP response pattern associated with the winter season $PC1_t$ (figure 6.1a) almost exactly resembles the pressure anomaly structure of the North Atlantic Oscillation (NAO).
An increase/decrease in the $PC1_t$ is associated with an increase/ decrease in pressure north of Iceland (low/high index NAO) and hence a decreased/ increased cold flow from north over Greenland.
Correlations between North Atlantic Nov-Apr SST and the winter season $PC1_t$ are presented in figure 6.2a. The pattern of correlations is almost identical to the SST versus NAO correlation pattern presented by Visbeck et al. [2003]. This again shows the solid relation between the winter time ice core $PC1_t$ and the NAO. The SST correlation pattern presented in figure 6.2a is believed to be a consequence of the NAO forcing of the SST [Visbeck et al. 2003].
The strong relation between the winter season $PC1_t$ and the winter season NAO is completely in line with the findings in the Vinther et al. [2003 a] paper (see figure A.2a in appendix A).
The $PC2_t$ related SLP structure is much weaker than the NAO related structure associated with the $PC1_t$. A change in the $PC2_t$ is associated with a flow change affecting the Greenland east coast. Hence an increase in the $PC2_t$ is related to a decrease in Scandinavian SLP leading to an enhanced cold flow from north along the Greenland east coast. This is in agreement

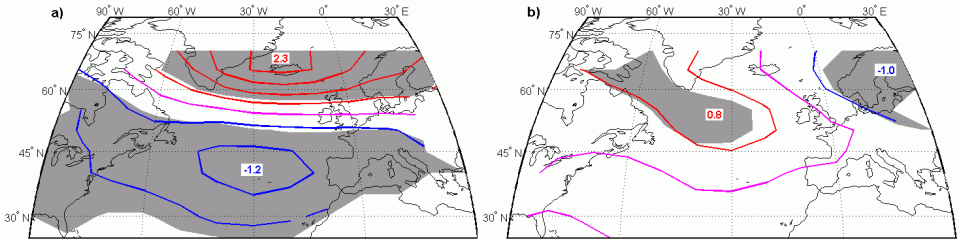

Figure 6.1: Spatial response patterns for Nov-Apr sea level pressure to a one σ increase in (a) the ice core winter season $PC1_t$, (b) the $PC2_t$. Patterns are determined using the period 1874-1970 and areas of grid point regression coefficients significantly different from zero are shaded. Contour intervals are 0.5hPa.

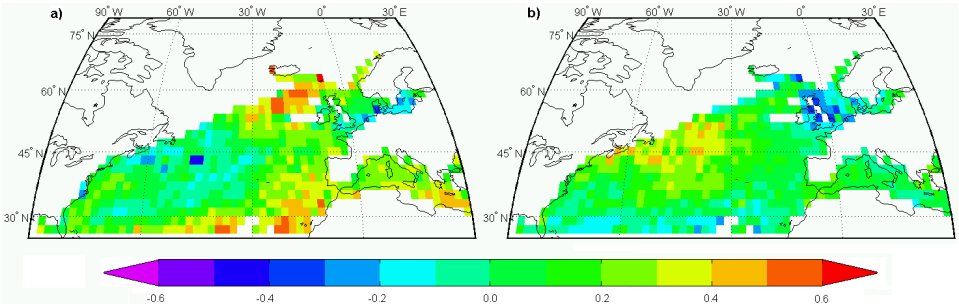

Figure 6.2: Correlations between Nov-Apr SST and the winter season ice core $PC1_t$ (a) and $PC2_t$ (b). Correlations are calculated for the period 1901-1970 and grid points with more than 60% missing values are left blank.

with the negative correlation between the $PC2_t$ and Tasiilaq Nov-Apr temperature (see table 5.5).
The SST correlation pattern associated with the winter season $PC2_t$ is presented in figure 6.2b. If a comparison is made with the SLP pattern associated with the $PC2_t$ (see figure 6.1b) it can be seen that the SST pattern probably is a result of the circulation pattern. The lower Scandinavian pressure is associated with increased advection of relatively cold air from north-west cooling the waters around the British Isles and Iceland. The higher pressure over the Labrador Sea will tend to reduce cold air outflow from eastern Canada and western Greenland, indirectly warming the Atlantic east of Newfoundland.

From figure 6.1 it can be seen that both the $PC1_t$ and $PC2_t$ are significantly associated with the SLP patterns over large (shaded) areas. The areas of significance were determined by calculation of correlation coefficients between grid point SLP and the ice core data. The 95% significance levels for the correlations are ± 0.2 [Bevington and Robinson, 1992].

No general significance levels can be given for the SST correlation patterns presented in figure 6.2, as the grid point correlations were calculated using differing numbers of years. Despite that fact, it is possible to give the very conservative estimate that all correlations larger than 0.4 or smaller than -0.4 are significant at least at the 95% level.

6.5 Obtaining spatial response patterns to summer season $\delta^{18}O$ variability

For the summer season the same approach was chosen as for the winter season, except that for summer, May-Oct SLP and SST averages were derived and a smaller contour interval was chosen for the SLP patterns as SLP variations are smaller during summer times. Finally it should be mentioned that the SLP data allowed for regressions to be carried out over the one year longer 1873-1970 period.

6.6 The summer season

The SLP response pattern associated with the summer season $PC1_t$ is shown in figure 6.3a. Surprisingly the summer $PC1_t$ seems to have only a very weak associated SLP structure. In fact there are almost no areas of the SLP structure made up of grid points with regression coefficients significantly different from zero.
In figure 6.4a correlations between the summer season $PC1_t$ and May-Oct SST are shown. The pattern generally show weak relations except for an area of positive correlations reaching from just south of Greenland to the waters around Iceland and north of the Faroe Isles.
The very week and probably insignificant SLP pattern shown in figure 6.3a is not likely to be able to force SST conditions. Hence the SST pattern associated with the summer season $PC1_t$ time series is probably due to the shifting SST conditions associated with drifting sea ice (along the Greenland east and south coast) and the changing position of the boundary between water of polar and Atlantic origin between Iceland and the Faroe Isles.
The SLP response associated with the summer $PC2_t$ is quite similar to that related with the winter season $PC2_t$ (see figures 6.3b). Some differences can be noted though. Most importantly the area of significant negative SLP response south-east of Newfoundland.
Correlations between SST and the summer season $PC2_t$ are presented in figure 6.4b. For the summer season a comparison with figure 6.3b suggests that the SST pattern very well could be related to the SLP pattern. Positive SST correlations are associated with higher than normal pressure bringing warmer than normal summer temperatures and vice versa.

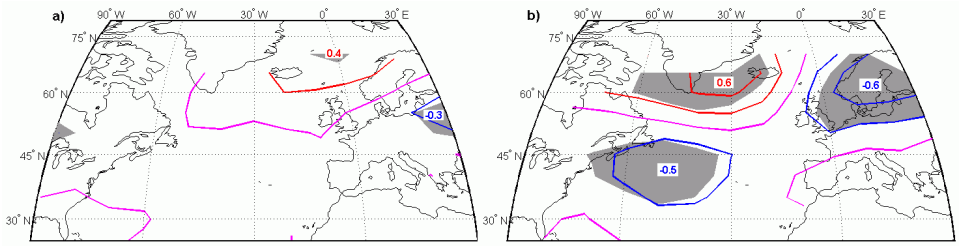

Figure 6.3: Spatial response patterns for May-Oct sea level pressure to a one σ increase in (a) the ice core summer season $PC1_t$, (b) the $PC2_t$. Patterns are determined using the period 1873-1970 and areas of grid point regression coefficients significantly different from zero are shaded. Contour intervals are 0.25hPa.

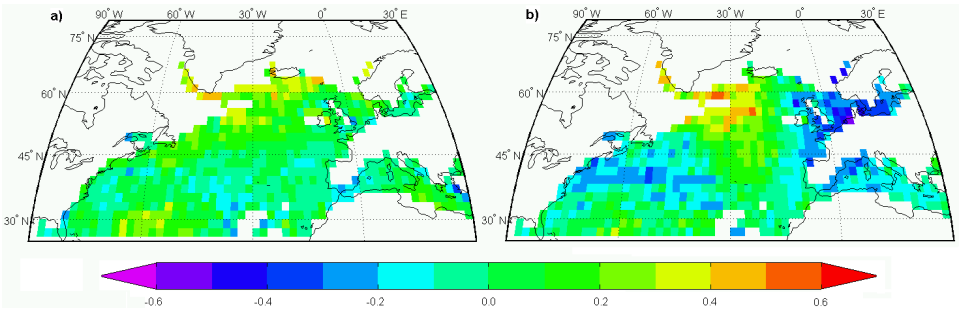

Figure 6.4: Correlations between May-Oct SST and the summer season ice core $PC1_t$ (a) and $PC2_t$ (b). Correlations are calculated for the period 1901-1970 and grid points with more than 60% missing values are left blank.

6.7 Summary

Patterns of North Atlantic region seasonal SST and SLP responses to changes in the time series of two first principal components of ice core seasonal $\delta^{18}O$ variability were presented.
The winter season $PC1_t$ was found to be strongly associated with the winter NAO, while the winter $PC2_t$ was related to Scandinavian pressure changes controlling flow that affects the Greenland east coast.
Winter season SST correlation patterns associated with the winter season ice core $PC1_t$ and $PC2_t$ could largely be explained by the SLP patterns forcing SST conditions.
No significant relations were found between SLP and the summer season ice core $PC1_t$. Hence the positive correlations between the summer season $PC1_t$ and May-Oct SST south of Greenland, around Iceland and north of the Faroe Isles, cannot be explained by an associated SLP pattern.
It is therefore speculated that the summer season ice core $PC1_t$ is directly linked to SST variability related to changes in sea ice conditions and variations in oceanic currents in a large area around Iceland.
It should be noted that sea ice conditions in the Denmark Strait and Greenland Sea as well as the position of the boundary between polar and Atlantic water masses are known to significantly influence icelandic temperatures.
That icelandic summer temperatures were related to the ice core $\delta^{18}O$ summer $PC1_t$ (see table 5.7) therefore supports this theory.
The summer season $PC2_t$ related SLP pattern was found to be very similar to the winter season $PC2_t$ related pattern. The SST correlation pattern associated with the summer $PC2_t$ was found to be associated with the corresponding SLP patter.

Chapter 7

The Stability of the Relations between Seasonal $\delta^{18}O$ and Atmospheric and Oceanic Conditions

In the previous chapter time series for the main principal components of seasonal ice core variability have been linked to different atmospheric flow patterns and SST structures in the North Atlantic region.
Importantly the winter $PC1_t$ was found to relate strongly to the NAO while the summer $PC1_t$ seemed to be associated with sea ice associated SST variability.
In this chapter the stability of these relations will be closer examined. If the Greenland ice core seasonal $\delta^{18}O$ data are to be used in reconstructions of past atmospheric and oceanic conditions, stable relations are of the utmost importance. Instabilities in the relations will unavoidably lead to erroneous interpretations of past climatic conditions.

7.1 The NAO and the winter season $PC1_t$

The NAO is the most important pattern of northern hemisphere atmospheric variability. Hence the desire to gain knowledge of past NAO conditions has been great.
The usual approach is to calculate an index of the NAO using pressure observations from each end of the so called NAO pressure seesaw, i.e. from Iceland and the Azores (or alternatively the Iberian peninsula).
Systematic pressure observations at these locations has however only been carried out for the past ~180 years [Jones et al., 1997; Vinther et al., 2003 b]. NAO index reconstructions based on early European observations of pressure and temperature reaches back to 1659 A.D. [Luterbacher et al., 1999;

Figure 7.1: Running 30 year correlations between the winter season ice core $PC1_t$ and November to April means of the Vinther et al. [2003 b] NAO index. Correlations numerically larger than 0.36 are significant at the 95% level.

2002], the year where the central England temperature record commenced [Manley, 1974].
In order to extend knowledge of the NAO beyond 1659 A.D. various NAO index reconstructions based on a variety of proxy data have been presented [Appenzeller et al., 1998 b; Cook et al., 1998; Stockton and Glueck, 1999]. Schmutz et al. [2000] did however thoroughly document the shortcomings of these reconstructions. None of them had stable relations with the [Luterbacher et al., 1999] observation based NAO reconstruction.
The findings of Schmutz et al. [2000] therefore clearly demonstrates the need for a thorough investigation into the stability of the relation between the NAO and the winter season $PC1_t$. An investigation carried out to examine the suitability of the winter $PC1_t$ for NAO reconstructing purposes. Using the same approach as Schmutz et al. [2000], 30 year running correlations were calculated between the ice core winter season $PC1_t$ and Nov-Apr means of the Vinther et al. [2003 b] NAO index (this index is a slightly improved version of the original Jones et al. [1997] NAO index).

From figure 7.1 it can be seen that the winter season $\delta^{18}O$ $PC1_t$ is significantly correlated to the Vinther et al. [2003 b] NAO index for almost all 30 year periods.
Note that correlations between the NAO index and the $PC1_t$ should be negative as high index NAO conditions are related to below normal Greenland winter temperatures.
The relations between the winter $PC1_t$ and the NAO are therefore remarkably stable. Especially if one compares the $PC1_t$ to other available NAO proxies [Schmutz et al. 2000].

7.1.1 Relations between the NAO and winter season $\delta^{18}O$ during the Late Maunder Minimum

Some of the ice cores used for deriving the winter season $PC1_t$ (in chapter 5) only spans some 200 years of accumulation. It is therefore not possible to investigate relations between the winter season $PC1_t$ and the NAO much further back in time than has already been done in figure 7.1.
In the Vinther et al. [2003 a] paper (appendix A) a smaller subset of ice cores were used than in chapter 5. These ice cores do however have the advantage that they all span some 700 years of accumulation, thus providing for NAO relations to be investigated far back in time.
As the research for this thesis progressed some shortcomings of the analysis made in the Vinther et al. [2003 a] paper did however become clear:

- As mentioned in chapter 4, the Dye 3 cores should not have been assumed to have stable annual $\delta^{18}O$ cycles.
- In chapter 5 shortcomings were found in the seasonal GRIP data.
- The sampling of the Renland ice core was found not to be of sufficient resolution for reliable seasonal information to be extracted from the core.

Despite of these findings the winter season $PC1_t$ from the Vinther et al. [2003 a] paper (from now on named the $PC1_t - V$) should still be a quite reliable proxy for Greenland winter temperatures at least before 1890 A.D. This is because of the following:

- The Vinther et al. [2003 a] PC1 only has little weight on the Renland (East) core (see table A.2).
- The annual cycle in the Dye 3 data stabilizes below some 60 meters of depth, which corresponds to an age of $\sim$ 80 years.
- Data from the mysterious GRIP 89-3 core were not used in the Vinther et al. [2003 a] paper.

It was therefore decided not to redo the quite extensive amount of calculations made for the Vinther et al. [2003 a] paper.
Instead of spending time on deriving a new $\sim$700 year long $PC1_t - V$ it was found more fruitful to focus on a remaining issue of Late Maunder Minimum (LMM) (A.D. 1675-1715) disagreements between the $PC1_t - V$ and the Luterbacher et al. [2002] NAO reconstruction (NAO-L).
From figure A.3 it can be seen that around the turn of the 17th century correlations between the NAO-L and $PC1_t - V$ approach zero. The correlation durring the 30 year period 1686-1715 being as modest as -0.11.
As there is no obvious reason to expect the ice core data to have problems in

Table 7.1: Frequency table of observed wind directions[a] in the Øresund area for Dec-Mar with less than 15% missing daily observations during the period 1675-1715. All frequencies are in %.

Year	SW	W	NE	E
1684[b]	19.8	7.2	17.1	15.3
1691	16.1	16.9	15.3	10.2
1692	19.7	14.5	17.9	12.8
1693	19.7	20.5	12.0	6.8
1694	17.4	19.0	12.4	4.1
1695	14.5	16.4	22.7	11.8
1696	38.1	16.1	8.5	7.6
1697	13.1	12.1	23.4	4.7
1709[c]	8.9	6.9	7.9	19.8

[a]Calculated from data set presented in Frydendahl et al. [1992].
[b]Observations first from Øresund later the Baltic Sea near Bornholm.
[c]Observations from the Great Belt area.

that specific period, it was decided to study the NAO-L further. From 1686 to 1715 the NAO-L relies heavily on European temperature observations. Only one, or for a few years two pressure records are available for the NAO reconstruction.
The disagreement between the $PC1_t - V$ and the NAO-L is mainly due to a few winters where the $PC1_t - V$ suggests very low Greenland winter temperatures while the NAO-L suggests low index NAO conditions, which are consistent only with above normal Greenland temperatures (see figure 1.1).
As the NAO-L is based mainly on western European temperature observations in the 1686-1715 period, it will suggest low index NAO conditions when these temperatures are below normal (see figure 1.1).
Is it possible to have below normal winter temperatures in Europe and Greenland at the same time? Common wisdom says no. The NAO winter temperature seesaw assures deviations of opposite sign at exactly these locations.
To avoid wasting time on an apparently hopeless theory of a weakening of the NAO temperature seesaw, it was decided to search for a third NAO related data set covering the 1686-1715 period. Hoping to clarify whether or not the $PC1_t - V$ really could be correct in its Greenland winter temperature estimates.

In Frydendahl et al. [1992] a large database of meteorological observations mainly from Danish naval vessels was presented. The observations were all from the period 1675-1715. According to Frydendahl et al. [1992] especially observations of wind direction should be reliable.

Table 7.2: Correlations between the Vinther et al. [2003] ice core PC1 time series ($PC1_t - V$) and the wind direction frequencies given in table 7.2.

SW	W	NE	E	(SW+W)-(NE+E)
-0.49	-0.39	0.35	0.60	-0.68[a]

[a]Correlation significant at the 95% level.

Over southern Scandinavia the winter time wind direction is strongly influenced by NAO conditions. NAO high index conditions are generally associated with south-westerly and westerly winds, while NAO low index conditions relates to easterly and north easterly winds.
Hence it was decided to calculate wind direction frequencies from the Frydendahl et al. [1992] data set. Wind direction frequencies for NAO relevant wind directions are shown in table 7.1.
Unfortunately only 9 years from the data set had sufficient observations during the entire Dec-Mar period for wind direction frequencies to be calculated (Dec-Mar was chosen as the $PC1_t - V$ is based on only 30% of the yearly data). Despite the few winters available for comparison table 7.2 shows that the $PC1_t - V$ is significantly correlated to the (ad hoc) NAO index defined by the wind direction frequency combination (SW+W)-(NE+E). Hence for these 9 years the $PC1_t - V$ seems to be significantly related to the NAO.

Having no reason whatsoever to distrust the $PC1_t - V$ during the 1686-1715 period after the positive verification against the old Danish wind observations, it was decided to give the theory of a weakening of the NAO winter temperature seesaw another chance.
Browsing through modern data, an interesting month was found: January 1984. This is one of the coldest months registered in the Greenland temperature records and a month of high index NAO conditions. But most importantly a month with negative temperature anomalies over the British Isles (see figure 7.2).
Hence it is possible, under extreme cold Greenland winter conditions, to have advection of colder than normal air from west to the British Isles.

The winters during the LMM, where the $PC1_t - V$ and NAO-L disagreed seems to have the same characteristics as the month of January 1984. The $PC1_t - V$ suggests very cold Greenland winter conditions, while the NAO-L suggests low index NAO based on slightly below normal temperatures in western Europe.
During the LMM severe sea ice conditions were observed around Iceland. It is therefore reasonable to assume that north Atlantic SST was somewhat below normal during the LMM.
Lower than normal SST would of course facilitate the scenario of cold air advection from west over the Atlantic. The very cold air originating from western Greenland would be less heated during its journey over the Atlantic.

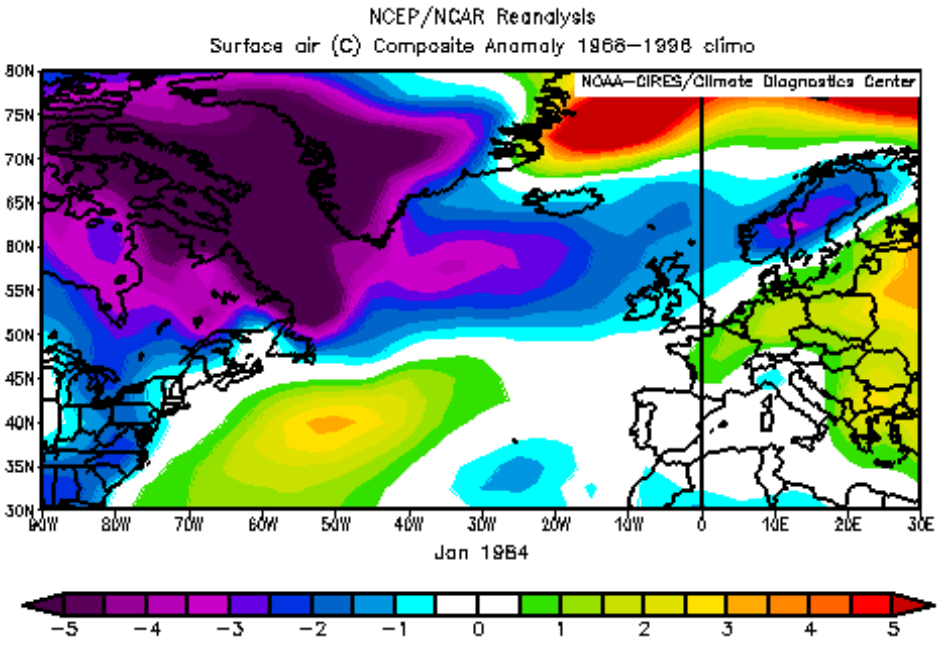

Figure 7.2: Temperature anomaly plot for January 1984 from the NCEP/NCAR reanalysis project [Kalney et al., 1996].

Therefore the air mass could have a temperature even further below normal than in January 1984 when reaching the British Isles and western parts of Europe.
There is therefore reason to believe that the disagreement between the NAO-L and the $PC1_t - V$ during the period 1686-1715 is due to a weakening of the NAO temperature seesaw affecting the ability of the NAO-L to correctly reconstruct the atmospheric flow.
This would imply that the $PC1_t - V$ is in fact a more stable proxy for the NAO than are European temperatures.
If that is the case, winter season $\delta^{18}O$ from Greenland ice cores must be concluded to be nearly ideal for reconstructing past NAO condition.

7.2 Stykkisholmur summer temperatures and the summer season $PC1_t$

Ideally the stability of the relations between the ice core summer season $PC1_t$ and SST conditions around Iceland and along the Greenland eastern and southern coasts should be verified over a long time period.
The small amount of SST observations in these areas does however not permit for such an analysis.

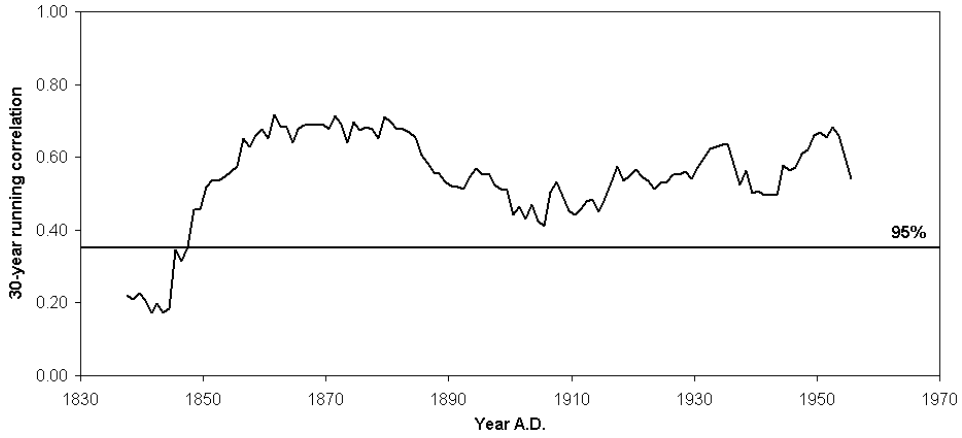

Figure 7.3: Running 30 year correlations between the summer season ice core PC1 time series and May to October means of Stykkisholmur temperature. Correlations larger than 0.36 are significant at the 95% level.

Instead of SST data it was therefore decided to use the long Stykkisholmur temperature series for the stability analysis. A choice being based on the fact that Stykkisholmur temperatures are related to the SST and sea ice conditions around Iceland.
Mimicking the stability analysis in the previous section, it was decided to calculate 30 year running correlations between Stykkisholmur May-Oct temperatures and the $PC1_t$ of summer season $\delta^{18}O$.
From figure 7.3 it can be seen that relations are indeed very stable except for a small period in the beginning of the record.
As the Stykkisholmur temperature record consists of adjusted observations from Reykjavik for the period 1823 to 1845 [Jonsson, 1989], it is probably a homogeneity problem in the early Stykkisholmur temperature record that causes the correlation to drop markedly there.
If only the period 1846 to 1970 is used for calculating the correlation between the summer $PC1_t$ and Stykkisholmur May to Oct temperatures, the correlation increases from the 0.49 given in table 5.8 to 0.55.
Relations between Stykkisholmur summer temperatures and the summer season $PC1_t$ are therefore probably stable and even stronger than expected. This could very well be an indication, that relations between SST conditions and the summer season $PC1_t$ are also strong and stable.

7.2.1 Summer season $\delta^{18}O$ during the Late Maunder Minimum

As was the case for the winter $PC1_t$, the summer $PC1_t$ only reaches some 200 years back in time. It is however possible to derive an almost 300 year long summer season $\delta^{18}O$ series stacked from the three Dye 3 71, 79 and 4B

Figure 7.4: Summer $\delta^{18}O$ values for the Dye 3 stack consisting of the 71, 79 and 4B cores.

cores.
The Dye 3 stacked summer $\delta^{18}O$ series does relate very well to Stykkisholmur temperatures. The correlation between May-Oct Stykkisholmur temperatures and the Dye 3 stack being 0.52 for the period 1846-1970. This relation is nearly as strong as the one between the summer $PC1_t$ and Stykkisholmur May-Oct temperatures for the same period.
The stacked series reaches back to the summer of 1692 A.D. and can therefore provide information on Icelandic summer temperature conditions during the last part of the LMM.

In figure 7.4 summer $\delta^{18}O$ values for the earliest part of the Dye 3 stack are shown. Interestingly values are low for the periods 1697 to 1700 and 1705 to 1707. This coincides with winters of major disagreement between the $PC1_t - V$ and the NAO-L. The winters being 1698/99, 1699/1700 and 1704/05.
If summer $\delta^{18}O$ indeed is related to SST conditions in an area around Iceland and south of Greenland as suggested by the findings in chapter 6, this implies that the winters of disagreement between the $PC1_t - V$ and the NAO-L all are in periods with below normal SST.
For all these winters the $PC1_t - V$ suggests very cold Greenland temperatures in contradiction to what is expected from the NAO-L.
The summer season $\delta^{18}O$ data from the Dye 3 stack therefore supports the theory of a weakening of the NAO winter temperature seesaw. The suggested cold SST conditions facilitating colder than normal air to be advected from a very cold Greenland region to western Europe during the winters of major disagreement between the $PC1_t - V$ and the NAO-L.

7.3 Summary

The relation between the NAO and the winter season $\delta^{18}O$ $PC1_t$ was examined and found to be remarkably stable.
Relations between Stykkisholmur summer temperatures and the summer season $\delta^{18}O$ $PC1_t$ were also found to be stable.
These stable relations suggests that the seasonal $\delta^{18}O$ data are suitable for detailed reconstructions of past climatic conditions.
Summer and winter $\delta^{18}O$ data from the Late Maunder Minimum (LMM) period were studied in detail. They painted a coherent picture of periods of colder than normal north Atlantic SST conditions leading to a weakening of the NAO temperature seesaw during the LMM.
The weakening was found to be a consequence of the possibility for very cold air of Greenland origin to flow over the relatively cold Atlantic waters without being heated sufficiently to bring above normal winter temperatures to western Europe.
These results seems to be reliable as winter $\delta^{18}O$ data were in line with wind direction observations from Danish naval vessels during the LMM.
The LMM analysis therefore indicates that a wealth of information about the climate of the past can be drawn from the seasonal $\delta^{18}O$ data.

Chapter 8

Discussion

During this survey many decisions and compromises have been made with regard to the processing and analysis of the ice core data. Even though careful considerations have been made in order to make this study as consistent as possible, unanswered questions will always remain. This discussion is devoted to further elaborate on such remaining issues.

In chapter 4 numerical methods were developed for diffusion correction. A more thorough analysis of the implications of filter length, high frequency cutoff and sampling density would be interesting. Consequences of ice core sampling method (constant sample thickness versus constant sample time span) should also be investigated. Especially because the GRIP cores are the only ice cores used, which have been cut into samples of equal thickness. Hence the problems with the GRIP cores discovered in chapter 5 could be related to the equal length sampling method.
In fact equal length sampling has the unfortunate implication that the annual $\delta^{18}O$ cycle will span different numbers of samples. This will tend to smear out the power off the annual cycle on a number of Fourier components when diffusion correcting the $\delta^{18}O$ data. Hence a stability analysis of the annual cycle in the diffusion corrected GRIP $\delta^{18}O$ data should have been carried out in chapter 4.
A quick examination of the annual cycle in the diffusion corrected GRIP 93 core does in fact yield power estimates ranging from $7.0‰^2$ to $17.0‰^2$. Much larger fluctuations than were seen in the ice cores cut into samples of constant time span. This clearly indicates that a further refinement of the diffusion correction method for equal length sampled $\delta^{18}O$ data is needed. It does however not explain the problems with annual GRIP $\delta^{18}O$ data discovered by White et al. [1997].
Another issue is the selection of seasonal data. In this survey it was decided to use 50% of the annual stable isotope data to define seasonal data. More sophisticated selection criteria might yield stronger associations between seasonal ice core data and climate. In fact it seems that relations

between winter season $\delta^{18}O$ and the NAO are somewhat stronger if only some 30% of the annual data are used. The choice made in the Vinther et al. [2003 a] paper.
In the Vinther et al. [2003 a] paper GRIP data were not excluded from the analysis. In chapter 5 it could have been decided only to exclude data from the problematic GRIP 89-3 ice core. One could argue that the weak relations between the $\delta^{18}O$ data and Greenland temperatures in itself shows that data from GRIP 89-3 ice core are suspect. As a more objective excuse for neglecting only the troublesome data could not be found, such a decision did however seem inappropriate.

Relations between the seasonal $\delta^{18}O$ data and sea level pressure (SLP) as well as sea surface temperatures (SST) in chapter 6 were found using quite recent data only (the latest 70-100 years in the ice cores). If seasonal $\delta^{18}O$ data are to be used for millennial scale climatic reconstruction projects, a longer period to ascertain relations would be preferable.
A comparison spanning a longer period was to a certain degree carried out in chapter 7. It is however somewhat disturbing that both the relation between the main component of winter season $\delta^{18}O$ data and the NAO, as well as the relation between summer season $\delta^{18}O$ and Icelandic summer temperatures seem to deteriorate in the early 19th century.
Even though the latter (far most dramatic) deterioration could be explained by a possible inhomogeneity in the Icelandic temperature record, it would indeed be comforting to verify the early 19th century relations further.
Some reassurance was provided though, by the convincing correspondence between Late Maunder Minimum (LMM) Danish wind direction observations and winter season $\delta^{18}O$ data.
The coherence between the winter and summer $\delta^{18}O$ data during the LMM in suggesting the optimal conditions for a weakening of the NAO temperature seesaw is also quite comforting. Such a weakening would explain the major disagreements between the Luterbacher et al. [2002] NAO reconstruction (NAO-L) and the winter season $\delta^{18}O$ data during the LMM.
The 9 winters covered by the old Danish wind data did unfortunately not coincide with any of the winters of major disagreement between the winter season $\delta^{18}O$ data and the NAO-L. Hence firm proof of the ability of the winter season $\delta^{18}O$ data to faithfully record NAO conditions during the LMM could not be given.
Serious questions on the ability of the NAO-L to interpret NAO conditions from European winter temperatures were however raised. Questions, which were backed up by modern data from the month of January 1984.
It therefore seems very likely that seasonal $\delta^{18}O$ data will indeed prove themselves as a powerful tool in future reconstruction efforts of climates of the past.
Indeed Luterbacher [pers. comm.] has decided to include Greenland ice core winter season $\delta^{18}O$ data in an upcoming NAO reconstruction.

Chapter 9

Conclusion

A thorough investigation of seasonal $\delta^{18}O$ in ice cores from the Greenland ice sheet has been carried out. Both the summer and winter season $\delta^{18}O$ signals were found to be related to seasonal Greenland and Iceland temperatures. Hence seasonal $\delta^{18}O$ can contribute to fulfill the desire of having seasonally resolved regional climate proxies.
Winter season $\delta^{18}O$ was found have both strong and stable relations to the North Atlantic Oscillation (NAO) during winter times. Since the NAO is the main pattern of northern hemisphere (NH) variability, obtaining information on past NAO conditions is a significant achievement in itself. Such information can clearly be obtained from winter season $\delta^{18}O$.
An analysis of the relations between the NAO and winter season $\delta^{18}O$ during the Late Maunder Minimum (1675-1715) did indeed suggest, that winter season $\delta^{18}O$ is more consistently related than European winter temperatures to the NAO. Summer season $\delta^{18}O$ was found to be associated with sea surface temperatures south of Greenland, in the Denmark Strait and just north of the Faroe Isles.
It is speculated that information about the state of the Greenland and Norwegian Seas could be provided by summer season $\delta^{18}O$ from Greenland ice cores. This would be of great importance for the study of the thermohaline circulation; a major research topic in the field of climate change.
Further investigations into this relation is however needed before firm conclusions can be drawn.
Significant relations between the main components of seasonal $\delta^{18}O$ and NH sea level pressure (SLP) were found. This suggests that the seasonal $\delta^{18}O$ could be helpful in the ongoing efforts to reconstruct past NH SLP variability.
In the process of retrieving the seasonal $\delta^{18}O$ from the highly resolved ice core data significant achievements were made. This includes the introduction of an enhanced simple ice flow model, as well as a new set of equations quantifying stable isotope diffusion in ice sheets.

Appendix A

NAO signal recorded in the stable isotopes of Greenland ice cores

B. M. Vinther, S. J. Johnsen, K. K. Andersen, H. B. Clausen and A. W. Hansen

Geophysical Research Letters, 30(7), 1387, doi:10.1029/2002GL016193, 2003.

Abstract

The winter $\delta^{18}O$ signal is extracted from 7 Greenland ice cores covering the past ~700 years. To filter out noise and local variations in the 7 isotope records a principal component analysis is carried out on the ice core data. A comparison between the time series of the first principal component (PC1) with 67 years of winter (December to March) temperature measurements from 3 southern Greenland synoptic stations shows highly significant correlations. Southern Greenland winter temperatures are known to be greatly influenced by the North Atlantic Oscillation (NAO). A good proxy for southern Greenland temperatures is therefore expected to reveal at least parts of the NAO signal. It is shown that the PC1 time series indeed is significantly correlated to the NAO during the winter months. The inclusion of ice core winter season $\delta^{18}O$ time series in future multiproxy NAO reconstructions is therefore recommended.

Introduction

The North Atlantic Oscillation (NAO) is known to have a large influence on climate in the North Atlantic region It is therefore desirable to extend

our knowledge of past variability of the NAO far back in time. However pressure measurements at the NAO's two centers of action (Iceland and the Azores/Iberia) are available for the last ~180 years only. Reconstructions of the NAO based on early European instrumental and documentary data reaches back to 1500 A.D. [Luterbacher et al., 1999; 2002] leaving documentary and natural proxies for meteorological data as the only means of reconstructing the NAO prior to around 1670 [Luterbacher et al., 2002].
In recent years a variety of annually resolved proxy based NAO indices has been presented, but only in a few cases [Glueck and Stockton, 2001; Cook et al, 2002] they reached back beyond 1500 A.D.
Greenland winter climate is known to be heavily influenced by the NAO and studies over the last 10 years show a connection between the NAO and climate records from Greenland ice cores [e.g. Barlow et al., 1993; White et al., 1997; Appenzeller et al., 1998 a; b and Rogers et al., 1998]. Rogers et al. [1998] showed that winter stable isotope data from central Greenland firn cores relates very well to the NAO during 29 winters (1959-1987). Appenzeller et al. [1998 a; b] found significant correlations between NAO indices and annual accumulation data from Greenland ice cores.
This paper presents a time series for mid to southern Greenland temperature spanning the winters from 1245 to 1970 A.D. The time series is so far the only available annually resolved proxy for the NAO reaching to the early 13th century. Principal component analysis and stacking are applied to winter season $\delta^{18}O$ data from 7 ice cores drilled in southern, western, eastern and central Greenland in order to obtain the time series. Methods that have already proven useful in isolating temperature related signals from multiple $\delta^{18}O$ ice core records [Fisher et. al, 1996].
An investigation of how the derived proxy temperature time series compares with the North Atlantic region circulation and temperature patterns is also presented.
Finally relations between the derived proxy temperature time series and two NAO indices will be examined. The two NAO indices are based on instrumental pressure data [Jones et al., 1997] (NAO-J) and a variety of early instrumental and documentary data [Luterbacher et al., 1999; 2002] (NAO-L) respectively.

Ice Core Isotope Data and Temperature

The isotopic ratio $\delta^{18}O$ measured in ice cores can be used as a temperature proxy because of the temperature dependent fractionation of oxygen isotopes, that takes place while moisture travels from its evaporation area to the Greenland ice sheet [Dansgaard, 1964; Johnsen et al., 1989]. Hence climate oscillations on long time scales such as glacial and interglacial periods as well as Dansgaard-Oeschger events are clearly identified from ice core $\delta^{18}O$ records. Determining temperature variations on annual and seasonal

Table A.1: Ice Core Characteristics

Ice Core	Elevation m a.s.l.	Latitude °N	Longitude °W	Mean air temp. in °C
Crete	3172	71.12	37.32	-30
Dye 3 71[a]	2480	65.18	43.83	-20
Dye 3 79	2480	65.18	43.83	-20
GRIP 89-1	3230	72.58	37.64	-32
GRIP 93	3230	72.58	37.64	-32
Milcent	2450	70.30	44.55	-22
Renland	2350	71.57	26.73	-18
Ice Core	**Accumulation m ice per year**	**Ice Core length in m**	**Oldest layer**	**Year core drilled**
Crete	0.30	404	554 A.D.	1974
Dye 3 71[a]	0.56	372	1244 A.D.	1971
Dye 3 79	0.56	2037	B.C.[b]	1979
GRIP 89-1	0.23	260	920 A.D.	1989
GRIP 93	0.23	230	1063 A.D.	1993
Milcent	0.53	398	1177 A.D.	1973
Renland	0.50	325	B.C.[b]	1988

[a]Youngest layer in Dye 3 71 main core is 1951. The nearby Dye 3 4B core is used for the years from 1951 to 1970.

[b]The core was drilled to bedrock. Oldest layers ~100,000 years old.

time scales is however complicated by the fact that $\delta^{18}O$ data are biased by accumulation, i.e. the temperature proxy is only recorded during precipitation events. Nevertheless Steffensen [1985] showed that when omitting temperature data from periods without precipitation, the $\delta^{18}O$ record from the Dye 3 ice core compares very well to Greenland coastal temperatures during the period 1980-1983 even on monthly time scales.
Using ice core $\delta^{18}O$ records dating back hundreds of years it is however not possible to make corrections for accumulation inhomogeneities. Although disregarding the effects of variations in accumulation obviously leads to noise in $\delta^{18}O$ based proxy temperature records, White et al. [1997] found a highly significant correlation coefficient of r=0.471 between a stacked central Greenland isotope record and ~100 years of coastal Greenland annually averaged temperatures. Even on seasonal time scales Barlow et al. [1997] and Rogers et al. [1998] found significant correlations between central Greenland isotope ice core records and temperature measured at Greenland coastal synoptic stations.

The Greenland Ice Core Data

Ice core data from 5 different drill sites in the southern half of Greenland have been analyzed: Crete, Dye 3, Milcent, Renland and Summit (2 cores from the Dye 3 area: Dye 3 79 and Dye 3 71 and 2 cores from the Summit area: GRIP 89-1 and GRIP 93) [Hammer et al., 1978; Johnsen et al., 1992 b; White et al., 1997]. Figure A.1 shows the location of the drill sites while table A.1 provides details concerning the ice cores. All cores reach at least 800 years back; except for the Dye 3 71 ice core where the oldest layer is from 1244. The youngest discernible winter in the Milcent core dates back to 1970.

The Role of Diffusion

Firn diffusion in the top ~55 meters of the ice cores tends to smooth out $\delta^{18}O$ seasonal variations [Johnsen et al., 1999]. Hence back-diffused $\delta^{18}O$ data is preferable in comparison with raw data when examining seasonal signals in the $\delta^{18}O$ records. We will therefore use back-diffused data whenever possible. The method of back-diffusion is however vulnerable to melt layers in the ice cores, forcing one to use raw $\delta^{18}O$ data for three ice cores (the two Dye 3 cores and the Renland core) containing several melt layers. Due to high accumulation at the Dye 3 and Renland drill sites (see table A.1) the annual cycle at these sites is less damped and back-diffusion thus not essential.

Extraction of the Winter Isotope Signal

The isotopic year is defined between two adjacent minima of the (back-diffused) isotope profile. We here chose to base winter $\delta^{18}O$ data on the first sixth of the $\delta^{18}O$ data from a given isotopic year and the last eighth of the year before. The mean of the winter $\delta^{18}O$ values is calculated for each year. Hence ~29% of the annual accumulation is used to define winter values.

Having extracted winter $\delta^{18}O$ means for each winter in each ice core for the period 1245-1970 (the time period covered by all the ice cores) we turn to principal component analysis (PCA) to isolate a common regional signal. To avoid biasing the PCA by the three cores from the central Greenland ice divide (Crete, GRIP 89-1 and GRIP 93) or the two Dye 3 cores, we chose to stack these into a "central" and a "southern" core respectively. Furthermore the linear trends (caused mostly by diffusive damping of the annual $\delta^{18}O$ cycle) are removed from all cores to avoid biasing.

The PCA is then carried out for the total time period covered by all four cores (the southern, western (Milcent), eastern (Renland) and central core) i.e. 726 years. The weights on the four cores when forming the principal components are given in table A.2. The table also shows the variance explained by each component. From table A.2 it can be seen that all four

ice cores contribute to the first principal component (PC1) with the same sign. Hence the time series of the PC1 represents a truly regional signal explaining 36% of the total variance in the four cores. Because the ice core $\delta^{18}O$ records have a red spectrum it is important to note that PCA applied to four noise series with approximately the same red spectrum as the ice cores would give a PC1 explained variance of only 32% [Fisher, 2002; pers. comm.]. The ice core PC1 is therefore not simply produced by noise.

Winter Isotope Data Compared to Northern Hemisphere Climate

Comparison of the PC1 Time Series with Greenland Temperature Data

To evaluate how well the time series of the PC1 captures southern Greenland winter (Dec-Mar; year of Jan) temperatures, three synoptic stations with records extending back to the late 19th century were selected for comparison: Tasiilaq, Ivittuut and Nuuk (station locations are shown in figure 1) [Frich et al., 1996; Peterson et al., 1997]. Pearson correlations between station temperatures and the PC1 time series can be seen in table 3 (To make intercomparison possible correlations were calculated only for 67 winters were measurements from all three stations were available; namely 1895-1966 except 1901, 1911, 1919, 1927 and 1928).
As a measure of the southern Greenland temperature a simple mean was calculated for the three synoptic stations. The correlation between the PC1 time series and this southern Greenland temperature (table A.3) is r=0.75. This suggests that the PC1 time series captures 56% of southern Greenland winter temperature variance.

Comparison with North Atlantic Region Winter Circulation

To investigate how changes in North Atlantic region surface circulation and temperature patterns relate to the PC1 time series, two gridded data sets from the Climatic Research Unit (CRU), Norwich, UK are used: The CRU 5 ° latitude by 10 ° longitude monthly mean sea level pressure data set [Jones,

Table A.2: Ice Core Weights on Principal Components

	PC1	PC2	PC3	PC4
East	0.10	0.98	0.07	0.17
West	0.60	-0.20	0.44	0.64
Central	0.65	0.05	0.21	-0.73
South	0.46	-0.01	-0.87	0.16
Var. exp.	36%	25%	22%	16%

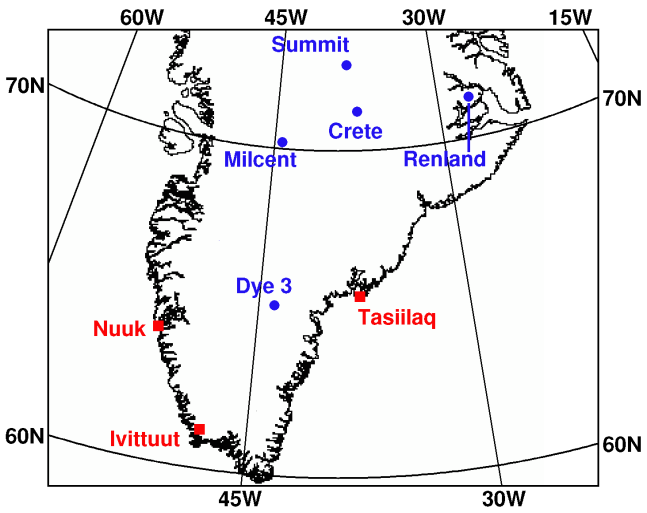

Figure A.1: Location of the Greenland ice core drill sites (blue) and temperature stations (red) used for this survey.

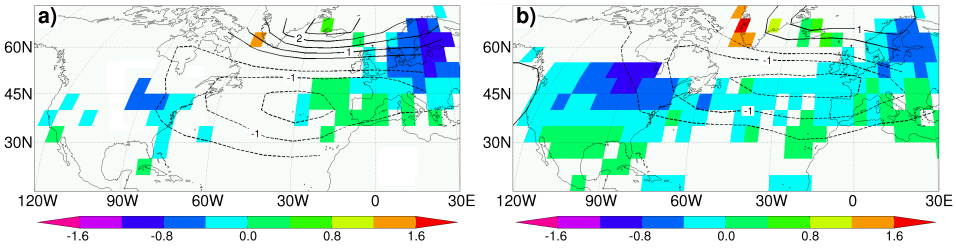

Figure A.2: The spatial response of surface pressure (contours in hPa) and temperature (scale in °C) corresponding to a 1σ increase in the ice core PC1 time series. (a) is based on a linear regression of the PC1 time series versus CRU Dec-Mar surface pressure and temperature data for 1874-1970 and 1857-1970 (year of Jan) respectively. (b) as for (a) but only for Dec-Mar 1897-1926 (see text for details). Grid points with more than 10% missing temperature data are left blank.

1987] (start January 1873) and the 5 ° by 5 ° "HADCRUT" temperature data set (start January 1856), that combines land and sea surface temperatures [Jones et al., 1999 b]. For each year Dec-Mar means are derived from the two CRU data sets and subsequently used to obtain spatial responses of surface pressure/temperature (figure A.2a) to a 1σ increase in the PC1 time series. The responses were calculated by means of linearly regressing grid point surface pressure/temperature against the PC1 time series.
It is clear that the North Atlantic region surface pressure response shown in figure A.2a compares very well to the NAO pressure structure (centers of action over Iceland and the Azores/Iberia). The surface temperature patterns found from the regression does also resemble NAO teleconnection patterns containing excursions of opposite sign in southern Greenland versus Europe and the eastern U.S.

Comparison with NAO Indices

For long term analysis of the connection between northern hemisphere winter circulation and the ice core PC1 time series a comparison with NAO indices is performed.
Pearson correlations between the PC1 time series and the NAO-J index as well as the NAO-L index are shown in table A.3. The PC1 time series is correlated at the 99.99% significance level (all significance levels are based on a standard t-table) to both NAO indices (Dec-Mar means) in the periods 1824-1970 for the NAO-J index and 1659-1970 for the NAO-L index.
As shown by Schmutz et al. [2000] correlations between NAO indices and proxy data such as the ice core based PC1 time series should be calculated not only for the maximum time period possible but also in smaller subperiods. This is to investigate the stability of the relation between a given proxy and the NAO. Hence 30 year running Pearson correlations between the PC1 time series and the two NAO indices are presented in figure A.3.
The PC1 time series is significantly correlated at the 95% level to the Dec-

Table A.3: Pearson Correlations between Climate Variables and the PC1 Time Series

Variable	Time Period	Correlation Coefficient
Ivittuut DJFM temperature	1895-1966	0.70[b]
Nuuk DJFM temperature	1895-1966	0.74[b]
Tasiilaq DJFM temperature	1895-1966	0.53[b]
Southern Gr. DJFM temperature[a]	1895-1966	0.75[b]
NAO-J index DJFM	1824-1970	-0.51[b]
NAO-L index DJFM	1659-1970	-0.45[b]

[a]Mean temperature at Ivittuut, Nuuk and Tasiilaq.
[b]Correlations significant at the 99.99% level.

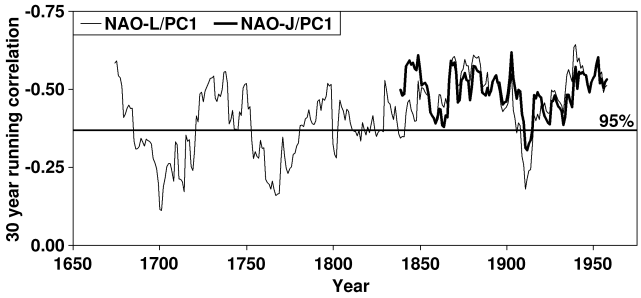

Figure A.3: Running 30 year Pearson correlations between the ice core PC1 time series and December to March means of the NAO-L and NAO-J indices. Correlations numerically larger than 0.36 are significant at the 95% level.

Mar mean NAO-J index for 116 out of a total of 120 30-year subsets. With regard to the Dec-Mar mean NAO-L index correlations are significant at the 95% level for 203 out of 285 30-year subsets. The non-significant correlations between the PC1 and the NAO-J for the 1896-1928 sub-periods could be a consequence of a weakened relation between the NAO and northern hemisphere surface temperatures during that period [Osborn et al., 1999]. It should however be noted that even in the sub-period 1897-1926 where the least significant correlation (r=-0.30) between the PC1 and the NAO-J is observed, surface pressure/temperature response patterns to changes in the PC1 time series still contain many NAO characteristics (see figure A.2b).

Conclusions

From Greenland ice core winter season $\delta^{18}O$ data it is possible to reconstruct more than half of the variance found in southern Greenland Dec-Mar mean temperatures during the period 1895-1966 using PCA techniques.
Linear regressions of North Atlantic region CRU data against the ice core based Greenland winter temperature reconstruction (the PC1 time series) are shown. The produced spatial response patterns of surface pressure and temperature resemble the known winter season NAO patterns.
Correlations between the PC1 time series and the NAO-J index are highly significant for the 1824-1970 period and significant for almost all 30-year sub-periods. Performance of the PC1 time series with regard to the NAO-L reconstructed index is slightly poorer. It is therefore not possible to determine whether the non-significant correlations between the PC1 time series and the NAO-L index in the early and late 18th century is caused by changes in the NAO teleconnections affecting Greenland (and thereby the PC1) or Europe (the NAO-L). In spite of the 18th century disagreements between the PC1 time series and the NAO-L index, they are however highly significantly correlated for the full period 1659-1970.

The recent multiproxy reconstruction of the NAO made by Cook et al. [2002] used a 90% significant correlation between a given proxy and a NAO-index (similar to the NAO-J) as an initial screening criterion for proxy records. The PC1 time series as well as each of the 7 ice core winter season $\delta^{18}O$ time series are all correlated to the NAO-J at the 95% level or better for the period 1824-1970. This combined with the good resemblance of NAO surface pressure and temperature patterns by the PC1 time series and the long time frame spanned by ice core data, makes the use of Greenland ice core winter season $\delta^{18}O$ data in future multiproxy NAO reconstructions very recommendable.

Acknowledgments

KKA thanks the Carlsberg foundation for financial support.

Appendix B

The Greenland Temperature Data

During the past decade multiple efforts have been made to obtain databases of homogeneous global/regional monthly temperature observations. The databases from which the Greenland temperature data has been obtained are: The Global Historical Climatology Network (GHCN) [Peterson and Vose, 1997], North Atlantic Climatological Dataset (NACD) [Frich et al., 1997], (NARP) [Jørgensen, 2001] and latest the report "The Observed Climate of Greenland, 1958-99" (TOCG) [Cappelen et al., 2001]. Unfortunately all these databases presently available are incomplete with regard to Greenland data. It has therefore been necessary to combine various sources in order to obtain as long time series of Greenland temperature observations as possible.
Combining temperature data from different databases is however somewhat problematic. In the creation of a given database specific techniques of homogenization have been used. This can lead to differences between databases in temperatures recorded for a given station.
Ideally a thorough investigation of the original observations and observation method should be carried out. This is however an immense task and far beyond the scope of this survey.
Here the temperature observations from the different sources will be combined by adjusting overlapping month of observation to have the same temperature.
Finally some of the gaps in the observation series will be filled by means of linearly regressing observations from neighboring stations.
Here follows a comprehensive list of the adjustments made to different monthly mean temperature records in compiling the final series.

Ilulissat (69.22°N, 51.05°W)

DATA SOURCES:

Jan 1840	-	Jun 1851	[Hann, 1890]	
Jul 1851	-	Dec 1856	No data	
Jan 1857	-	Dec 1865	[Hann, 1890]	Data adjusted from Uummannaq
Jan 1866	-	Dec 1872	GHCN	
Jan 1873	-	Dec 1960	NARP	
Jan 1961	-	Dec 1970	TOCG	

REMARKS:
Hann [1890] used Uummannaq (70.7°N, 52.0°W) data to fill some of the gap in the early Ilulissat series. Hann [1890] used a part of the Uummannaq series that overlapped Ilulissat observations (1866-1870) in order to homogenize the data. As this period of Uummannaq data could not be located, the Hann [1890] data was used without further verification.
All pre 1873 data had to be slightly adjusted in order to be in agreement with the later NARP and TOCG data. Adjustments used (in °C): Jan: 0.0, Feb: -0.1, Mar: 0.0, Apr: -0.4, May: 0.0, Jun: -0.8, Jul: -0.7, Aug: -0.7, Sep: -0.1, Oct: 0.1, Nov: 0.1 and Dec: 0.0.

Ivittuut (61.20°N, 48.20°W)

DATA SOURCES:

Jan 1873	-	Dec 1889	NARP	
Jan 1890	-	Sep 1918	NACD	
Oct 1918	-	Jun 1919	No data	
Jul 1919	-	Jan 1927	NACD	
Feb 1927	-	May 1928	No data	
Jun 1928			NACD	
Jul 1928			No data	
Aug 1928	-	Dec 1960	NACD	
Jan 1961	-	Aug 1966	GHCN	
Sep 1966	-	Dec 1970	GHCN	Data regressed from Kangilinnguit

REMARKS:
All pre 1889 data had to be adjusted in order to be in agreement with the later NACD and GHCN data. The data difference is due to an effort in the NARP data to combine Ivittuut observations with later observations at the quite distant Narsarsuaq meteorological station (61.17°N, 45.42°W). Adjustments used (in °C): Jan: 1.6, Feb: 1.6, Mar: 0.0, Apr: 0.0, May: 0.0, Jun: 0.1, Jul: 0.1, Aug: 0.1, Sep: 0.6, Oct: 0.6, Nov: 0.6 and Dec: 1.6.
In the NARP data set all the missing values in 1918/19 and 1927/28 has been filled in. The infilled values are however not observations, but slightly

adjusted climatological norms and therefore not of value for this survey.
The overlapping period (Jan 1961 - Aug 1966) between the Kangilinnguit ($61.22°N$, $48.12°W$) and Ivittuut observations has been used for linearly regressing (for each month of the year) the later Kangilinnguit observations to the Iviituut observations. It should be noted however that examination of the overlapping period suggest that Kangilinnguit observations are best related to Ivittuut observations in Sep-Apr. The regressed summer months (May-Aug, 1967-1970) should therefore only be used carefully on a month by month basis, but are of sufficient quality for seasonal means to be extracted.

Nuuk ($64.17°N$, $51.75°W$)

DATA SOURCES:

Jan 1866	-	Sep 1866	GHCN	
Oct 1866			No data	
Nov 1866	-	Oct 1884	GHCN	
Nov 1884	-	Jan 1885	DMI Yearbooks	Data regressed from Qoornoq
Feb 1885			GHCN	
Mar 1885			DMI Yearbooks	Data regressed from Qoornoq
Jul 1885	-	Dec 1889	GHCN	
Jan 1890	-	May 1896	NARP	
Jun 1896			GHCN	
Jul 1896	-	Mar 1899	NARP	
Apr 1899	-	May 1899	DMI Yearbooks	Data regressed from Qoornoq
Jun 1899	-	Sep 1900	NARP	
Oct 1900			GHCN	
Nov 1900	-	Dec 1900	NARP	
Jan 1901	-	Feb 1901	GHCN	
Mar 1901	-	Aug 1920	NARP	
Sep 1920	-	Oct 1920	GHCN	
Nov 1920	-	Dec 1957	NARP	
Jan 1958	-	Dec 1970	TOCG	

REMARKS:
All GHCN data had to be slightly adjusted in order to be in agreement with later NARP and TOCG data. Adjustments used (in $°C$): Jan: -0.1, Feb: 0.0, Mar: -0.1, Apr: -0.2, May: -0.3, Jun: -0.6, Jul: -0.4, Aug: -0.1, Sep: -0.1, Oct: -0.1, Nov: 0.1 and Dec: -0.1.
All monthly temperature data from the Yearbooks of the Danish Meteorological Institute (DMI) for the station of Qoornoq ($64.4°N$, $51°W$) were digitized (1874-1960). This station is very close to Nuuk and the correlation between monthly temperatures at the two observation sites are always in between 0.75 (Aug) and 0.96 (Dec and Feb) for the overlapping months. It is therefore quite safe to fill in the few missing months with regressed values

from Qoornoq.
In the NARP an GHCN data sets a number of different monthly values were left out. As comparison with Qoornoq temperatures strongly supported their validity, they were all included here.

Tasiilaq (65.60°N, 37.63°W)

DATA SOURCES:

Nov 1894	-	Aug 1910	NARP
Sep 1910	-	Aug 1911	No data
Sep 1911	-	Jul 1924	NARP
Aug 1924			No data
Sep 1924	-	Jun 1937	NARP
Jul 1937			No data
Aug 1937	-	Dec 1957	NARP
Jan 1958	-	Dec 1970	TOCG

REMARKS:
No further remarks.

Upernavik (72.78°N, 56.17°W)

DATA SOURCES:

Jan 1873	-	Nov 1873	NARP
Dec 1873			No data
Jan 1874	-	Dec 1957	NARP
Jan 1958	-	Dec 1970	TOCG

REMARKS:
The temperature for Dec 1873 was noted as being 0.1°C, an exceptional high temperature for a winter month. As the temperature for Dec 1873 at the nearest available station (Ilulissat) was recorded to be -14.7°C, the Upernavik temperature is completely unrealistic and was therefore rejected.

Appendix C

Drill Site Pressure Calculations

For most locations on the Greenland ice sheet, no or only very few pressure observations are available.
During the period from July 1989 to October 1996 a reasonable number of pressure observations were made at the GISP2 ($72.58°N$, $38.46°W$, elevation 3205 meters) ice core drill site by automatic weather stations (AWS) [Stearns, 1996].
The mean annual pressure calculated for months with less than 10% missing observations during the July 1989 to October 1996 period is 665.9 hPa for the GISP2 site.
All the drill site pressures presented in table 2.2 are estimated from the GISP2 mean pressure. Having a given drill site, the height difference between the drill site and the GISP2 site as well as the mean temperature for the two sites were calculated. These two parameters were subsequently used for calculating the pressure difference assuming hydrostatic balance and zero humidity.
This is off course a very crude method, but given the limited number of observations available from the Greenland ice sheet, further analysis seemed futile.

Appendix D

The Maximum Entropy Method

The maximum entropy method (MEM) can be viewed as a sophisticated procedure to estimate parameters for an autoregressive (AR) model.
Looking at AR modelling as a linear prediction problem is a simple way to approach MEM. This will be done here.
Assume that we have a time series of length M:

$$s_1, s_2, s_3, \ldots, s_M \tag{D.1}$$

The AR modelling will then use m parameters (where m<M) to try to predict a given value in the series from the m preceding values:

$$s_i(pred) = \sum_{j=1}^{m} s_{i-j} a_j \tag{D.2}$$

Here $a_1, a_2, ..., a_m$ are the parameters of the m'th order AR model.
The forward prediction error (f_i) of the AR model estimate is defined as:

$$f_i = s_i - s_i(pred) = s_i - \sum_{j=1}^{m} s_{i-j} a_j \tag{D.3}$$

The AR model can also be applied to the series backwards:

$$s_i(back - pred) = \sum_{j=1}^{m} s_{i+j} a_j \tag{D.4}$$

Which gives rise to the definition of the backward prediction error (b_i):

$$b_i = s_i - s_i(back - pred) = s_i - \sum_{j=1}^{m} s_{i+j} a_j \tag{D.5}$$

The mean error (E) of the AR model can then be defined as:

$$E = \frac{1}{2(M-m)} \left(\sum_{i=m+1}^{M} f_i + \sum_{i=1}^{M-m} b_i \right) \tag{D.6}$$

The MEM seeks to determine the m parameters in the AR model in such a manner that E is minimized.
In Andersen [1974] fast algorithms for determination of the AR model parameters can be found.

Assuming that the series given in (D.1) is in fact a series of equally spaced measurements with spacing Δt, then the power spectrum of the series can be determined [Andersen, 1974]:

$$P(f) = \frac{E\Delta t}{\left| 1 - \sum_{n=1}^{m} a_n e^{-2\pi i f m \Delta t} \right|^2} \tag{D.7}$$

Where f is the frequency and $i^2 = -1$. The mean error of the AR model (E) is also provided by the Andersen [1974] algorithm.
Determination of the power of peaks in the power spectrum can be done by numerical integration of the spectrum defined by (D.7).
Johnsen and Andersen [1978] did however find an alternative and more reliable method to evaluate spectral power. This method is the one used for this spectral peak power estimation in this thesis. For method details see [Johnsen and Andersen, 1978].

Here it will suffice to point out that when the number (m) of AR model parameters is increased, the power spectrum will be able to resolve more and more details. While decreasing m will give a more and more smooth power spectrum.
Correspondingly the Johnsen and Andersen [1978] power estimation technique will be able to resolve power in spectral peaks with closer and closer frequency as m is increased.
When analyzing the ice core data the resolution flexibility of MEM can be very useful. As an example it can be mentioned, that for a low m the annual cycle in $\delta^{18}O$ can be clearly seen as one spectral peak, despite being smeared over several different frequencies due to differences in precipitation between different years.

Bibliography

[1] Andersen, N., On the calculation of filter coefficients for maximum entropy spectral analysis, *Geophysics*, *39*, 69–72, 1974.

[2] Appenzeller, C., J. Schwander, S. Sommer and T. F. Stocker, The North Atlantic Oscillation and its imprint on precipitation and ice accumulation in Greenland, *Geophys. Res. Lett. 25*, 1939–1942, 1998.

[3] Appenzeller, C., T. F. Stocker and M. Anklin, North Atlantic Oscillation dynamics recorded in Greenland ice cores, *Science*, *282*, 446–449, 1998.

[4] Barlow, L. K., J. W. C. White, R. G. Barry, J. C. Rogers and P. M. Grootes, The North Atlantic Oscillation signature in deuterium and deuterium excess signals in the Greenland Ice Sheet Project 2 ice core, 1840-1970, *Geophys. Res. Lett.*, *20*, 2901–2904, 1993.

[5] Barlow, L. K., R. G. Berry, J. C. Rogers and M. C. Serreze, Aspects of climate variability in the North Atlantic Sector: Discussion and relation to the Greenland Ice Sheet Project 2 high resolution isotopic signal, *J. Geophys. Res.*, *C12*, 26,333–26,344, 1997.

[6] Bevington, P. R. and D. K. Robinson, Data reduction and error analysis for the physical sciences, Second Edition, Mc-Graw-Hill Inc, New York, USA, 348pp., 1992.

[7] Cappelen, J., B. V. Jørgensen, E. V. Laursen, L. S. Stannius and R. S. Thomsen, The Observed Climate of Greenland, 1958-99 - with Climatological Standard Normals, 1961-90, Technical Report 00-18 from the Danish Meteorological Institute, 2001.

[8] Clausen, H. B., N. S. Gundestrup and S. J. Johnsen, Glaciological investigations in the Crête area, central Greenland: A search for a new deep-drilling site, *Ann. Glaciol.*, *10*, 10–15, 1988.

[9] Clausen, H. B., and C. U. Hammer, The Laki and Tambora eruptions as revealed in Greenland ice cores from 11 locations, *Ann. Glaciol.*, *10*, 16–22, 1988.

[10] Cook, E. R., K. R. Briffa and P. D. Jones, Spatial regression methods in dendroclimatology: A review and comparisom of two techniques, *Int. J. Climatol.*, *14*, 379–402, 1994.

[11] Cook, E. R., R. D. D'Arrigo and K. R. Briffa, A reconstruction of the North Atlantic Oscillation using tree-ring chronologies from North America and Europe, *The Holocene*, *8*, 9–17, 1998.

[12] Cook, E. R., R. D. D'Arrigo and M. E. Mann, A Well-Verified, Multiproxy Reconstruction of the Winter North Atlantic Oscillation Index since A.D. 1400, *J. Climate*, *15*, 1754–1764, 2002.

[13] Dansgaard, W., Stable isotopes in precipitation, *Tellus*, *16/4*, 436–468, 1964.

[14] Dansgaard, W. and S. J. Johnsen, A flow model and a time scale for the ice core from Camp Century, Greenland, *J. Glaciol.*, *8*, 215–223, 1969.

[15] Dansgaard, W., S. J. Johnsen, H. B. Clausen and N. Gundestrup, Stable isotope glaciology Greenland, *Medd. om Grønland*, *197*, No. 2, 1–53, 1973.

[16] Dansgaard, W., S. J. Johnsen, H. B. Clausen, D. Dahl-Jensen, N. Gundestrup, C. U. Hammer, C. S. Hvidberg, J. P. Steffensen, Á. E. Sveinbjörnsdóttir, J. Jouzel and G. Bond, Evidence for general instability of past climate from a 250-kyr ice-core record, *Nature*, *364*, 218–220, 1993.

[17] Elms, J.D., S.D. Woodruff, S.J. Worley, and C. Hanson, Digitizing Historical Records for the Comprehensive Ocean-Atmosphere Data Set (COADS). *Earth System Monitor*, *2*, 4–10, 1993.

[18] Fisher, D. A., N. Reeh and H. B. Clausen, Stratigraphic noise in time series derived from ice cores, *Ann. Glaciol.*, *14*, 76–86, 1985.

[19] Fisher, D. A., R. M. Koerner, K. Kuivinen, H. B. Clausen, S. J. Johnsen, J. P. Steffensen, N. Gundestrup and C. U. Hammmer, Intercomparison of Ice Core $\delta^{18}O$ and Precipitation Records from Sites in Canada and Greenland over the last 3500 years and over the last few Centuries in detail using EOF Techniques, *NATO ASI Series*, Vol. 141, 297–328, 1996.

[20] Fisher, D. A., High-resolution multiproxy climatic records from ice cores, tree-rings, corals and documentary sources using eigenvector techniques and maps: assessment of recovered signal and errors, *The Holocene*, *12*, 401–419, 2002.

[21] Frich, P., H. Alexandersson, J. Ashcroft, B. Dahlström, G. R. Demarée, A. F. V. van Engelen, E. J. Førland, I. Hanssen-Bauer, R. Heino, T. Jónsen, K. Jonasson, L. Keegan, P. Ø. Nordli, T. Schmith, P. Steffensen, H. Tuomenvirta and O. E. Tveito, North Atlantic Climatological Dataset (NACD Version 1) - Final Report, Scientific Report 96-1 from the Danish Meteorological Institute, 1996.

[22] Frydendahl, K., P. Frich and C. Hansen, Danish Weather Observations 1675-1715, Technical Report 92-3 from the Danish Meteorological Institute, 1992.

[23] Glueck, M. F., and C. W. Stockton, Reconstruction of the North Atlantic Oscillation, 1429-1983, *Int. J. Climatol.*, *21*, 1453–1465, 2001.

[24] Hammer, C. U., H. B. Clausen, W. Dansgaard, N. Gundestrup, S. J. Johnsen and N. Reeh, Dating of Greenland ice cores by flow models, isotopes, volcanic debris, and continental dust, *J. Glaciol.*, *20*, 3–26, 1978.

[25] Hann, J., Zur Witterungsgeschichte von Nord-Grönland, Westküste, *Met. Zeit.*, *3*, 109–115, 1890.

[26] Hansen, A. W., B. M. Vinther, R. Vildhøj, Den lille istid - NAO eller fakta? En vigtig brik i forståelsen af den globale opvarmning, *Kvant*, *4*, 29–32, 2001.

[27] Herron, M. M. and C. C. Langway Jr., Firn densification: An empirical model, *J. Glaciol.*, *25*, 373–385, 1980.

[28] Hurrel, J. W., Y. Kushnir, G. Ottersen and M. Visbeck, An Overview of the North Atlantic Oscillation , *Geophysical Monograph.*, *134*, 1–35, 2003.

[29] Johnsen, S. J., Stable isotope homogenization of polar firn and ice, in *Proc. Symp. on Isotopes and Impurities in Snow and Ice, I.U.G.G. XVI, General Assembly, Genoble, 1975*, 210–219, Washington D.C., 1977.

[30] Johnsen, S. J. and N. Andersen, On power estimation i maximum entropy spectral analysis, *Geophysics*, *4*, 681–690, 1978.

[31] Johnsen, S. J., W. Dansgaard and J. W. C. White, The origin of Arctic precipitation under present and glacial conditions, *Tellus*, *41B*, 452–468, 1989.

[32] Johnsen, S. J. and W. Dansgaard, On flow model dating of stable isotope records from Greenland ice cores, *NATO ASI Series*, Vol. I 2, 13–24, 1992.

[33] Johnsen, S. J., H. B. Clausen, W. Dansgaard, K. Fuhrer, N. Gundestrup, C. U. Hammer, P. Iversen, J. Jouzel, B. Stauffer and J. P. Steffensen, Irregular glacial interstadials recorded in a new Greenland ice core, *Nature, 359*, 311–313, 1992.

[34] Johnsen, S. J., H. B. Clausen, W. Dansgaard, N. S. Gundestrup, C. U. Hammer, U. Andersen, K. K. Andersen, C. S. Hvidberg, D. Dahl-Jensen, J. P. Steffensen, H. Shoji, Á. E. Sveinbjörnsdóttir, J. White, J. Jouzel and D. Fisher, The $\delta^{18}O$ record along the Greenland Ice Core Project deep ice core and the problem of possible Eemian climatic instability, *J. Geophys. Res., C12*, 26,397–26,410, 1997.

[35] Johnsen, S. J., H. B. Clausen, J. Jouzel, J. Schwander, Á. E. Sveinbjörnsdóttir and J. White, Stable Isotope Records from Greenland Deep Ice Cores: The Climate Signal and the Role of Diffusion, *NATO ASI Series*, Vol. 156, 89–107, 1999.

[36] Johnsen, S. J., H. B. Clausen, K. M. Cuffey, G. Hoffmann, J. Schwander and T. Creyts, Diffusion of stable isotopes in polar firn and ice: the isotope effect in firn diffusion, in *Physics of Ice Core Records*, 121–140, Sapporo, 2000.

[37] Jones, P. D., The early twentieth century Arctic High - fact or fiction?, *Clim. Dyn., 1*, 63–75, 1987.

[38] Jones, P. D., T. Jonsson and D. Wheeler, Extension to the North Atlantic Oscillation using early instrumental pressure observations from Gibraltar and south-west Iceland, *Int. J. Climatol., 17*, 1433–1450, 1997.

[39] Jones, P. D., T. D. Davies, D. H. Lister, V. C. Slonosky, T. Jónsson, L. Bärring, P. Jönsson, P. Maheras, F. Kolyva-Machera, M. Barriendos, J. Martin-Vide, R. Rodriguez, M. J. Alcoforado, H. Wanner, C. Pfister, J. Luterbacher, R. Rickli, E. Schuepbach, E. Kaas, T. Schmith, J. Jacobeit and C. Beck, Monthly mean pressure reconstruction for Europe for the 1780-1995 period, *Int. J. Climatol., 19*, 347–364, 1999.

[40] Jones, P. D., M. New, D. E. Parker, S. Martin and I. G. Rigor, Surface air temperature and its changes over the past 150 years, *Rev. Geophys., 37*, 173–199, 1999.

[41] Jones, P. D., T. J. Osborn and K. R. Briffa, The evolution of climate over the last millinium, *Science., 292*, 662–667, 2001.

[42] Jonsson, T., The observations of Jon Thorsteinsson in Nes and Reykjavik 1820-1854, *Icel. Met.Office Report*, 1989.

[43] Jørgensen, P. V., Nordic Climate Data Collection 2001 - An update of: NACD, REWARD, NORDKLIM and NARP datasets, 1873-2000, Version 0, Technical Report 01-20 from the Danish Meteorological Institute, 2001.

[44] Kalney, E. and et al., The NCEP/NCAR Reanalysis 40-year Project, *Bull. Amer. Meteorol. Soc.*, *77*, 437–471, 1996.

[45] Langway Jr, C. C., H. Oeschger and W. Dansgaard, The Greenland ice sheet program in perspective, in: *Greenland Ice Cores: Geophysics, Geochemimistry and Environment.*, *AGU Monograph*, *33*, 1–8, 1985.

[46] Luterbacher, J., C. Schmutz, D. Gyalistras, E. Xoplaki and H. Wanner, Reconstruction of Monthly NAO and EU Indices back to AD 1675, *Geophys. Res. Lett.*, *26*, 2745–2748, 1999.

[47] Luterbacher, J., E. Xoplaki, D. Dietrich, P. D. Jones, T. D. Davis, D. Portis, J. F. Gonzalez-Rouco, H. von Storch, D. Gyalistras, C. Casty and H. Wanner, Extending North Atlantic Oscillation reconstructions back to 1500, *Atmos. Sci. Lett.*, *2*, 114–124, 2002.

[48] Manley, G., Central England Temperatures: monthly means 1659 to 1973, *Ouart. J. Roy. Met. Soc.*, *100*, 389–405, 1974.

[49] Merlivat, L. and J. Jouzel, Global Climatic Interpretation of the Deuterium-Oxygen 18 Relationship for Precipatation, *J. Geophys. Res.*, *C8*, 5029–5033, 1979.

[50] Osborn, T. J., K. R. Briffa, S. F. B. Tett, P. D. Jones and R. M. Trigo, Evaluation of the North Atlantic Circulation as simulated by a coupled climate model, *Clim. Dyn.*, *15*, 685–702, 1999.

[51] Peterson, T. and R. S. Vose, An overview of the Global Historical Climatology Network temperature database, *Bull. Amer. Meteorol. Soc.*, *78*, 2837–2849, 1997.

[52] Reeh, N., H. B. Clausen, W. Dansgaard, N. Gundestrup, C. U. Hammer and S. J. Johnsen, Secular trends of accumulation rates at three Greenland stations, *J. Glaciol.*, *20*, 27–30, 1978.

[53] Rogers, J. C., J. F. Bolzan and V. A. Pohjola, Atmospheric circulation variability associated with shallow-core seasonal isotopic extremes near Summit, Greenland, *J. Geophys. Res.*, *D10*, 11,205–11,219, 1998.

[54] Schmutz, C., J. Luterbacher, D. Gyalistras, E. Xoplaki and H. Wanner, Can we trust proxy-based NAO index reconstructions?, *Geophys. Res. Lett.*, *8*, 1135–1138, 2000.

[55] Slutz, R.J., S.J. Lubker, J.D. Hiscox, S.D. Woodruff, R.L. Jenne, D.H. Joseph, P.M. Steurer, and J.D. Elms, Comprehensive Ocean-Atmosphere Data Set; Release 1. NOAA Environmental Research Laboratories, Climate Research Program, Boulder, CO, 268 pp. (NTIS PB86-105723), 1985.

[56] Stearns, C., Automated weather station data for Greenland ice core locations. Boulder, CO: National Snow and Ice Data Center. Digital media, 1996.

[57] Steffensen, J. P., Microparticles in snow from the South Greenland ice sheet, *Tellus*, *37B*, 286–295, 1985.

[58] Stockton, C. W. and M. F. Glueck, Long-term variability of the North Atlantic Oscillation (NAO), *Proceedings of the Amarican Meteorological Society, Tenth Symposium on Global Change Studies,*, January 11-15, 1999, Dallas, TX, 290–293, 1999.

[59] Vinther, B. M., S. J. Johnsen, K. K. Andersen, H. B. Clausen and A. W. Hansen, NAO signal recorded in the stable isotopes of Greenland ice cores, *Geophys. Res. Lett.*, *30*(7), 1387, doi:10.1029/2002GL016193, 2003.

[60] Vinther, B. M., K. K. Andersen, A. W. Hansen, T. Schmith and P. D. Jones, Improving the Gibraltar/Reykjavik NAO Index, *Geophys. Res. Lett.*, Under review, 2003.

[61] Visbeck, M., E. P. Chassignet, R. G. Curry, T. L. Delworth, R. R. Dickson and G. Krahmann, The Ocean's Response to North Atlantic Oscillation Variability, *Geophysical Monograph.*, *134*, 113–145, 2003.

[62] White, J. W. C., L. K. Barlow, D. Fisher, P. Grootes, J. Jouzel, S. J. Johnsen, M. Stuiver and H. Clausen, The climate signal in the stable isotopes of snow from Summit, Greenland: Results of comparisons with modern climate observations, *J. Geophys. Res.*, *102*, 26,425–26,439, 1997.

[63] Woodruff, S.D, COADS updates including newly digitized data and the blend with the UK Meteorological Office Marine Data Bank and Quality control in recent COADS updates, Proceedings of Workshop on Preparation, Processing and Use of Historical Marine Meteorological Data, Tokyo, Japan, 9–13 and 49–53, 2001